Topology Reconfiguration To Improve The Photovoltaic (PV) Array Performance

by

Santoshi Tejasri Buddha

A Thesis Presented in Partial Fulfillment
of the Requirements for the Degree
Master of Science

Approved November 2011 by the
Graduate Supervisory Committee:

Andreas Spanias, Co-Chair
Cihan Tepedelenlioglu, Co-Chair
Junshan Zhang

ARIZONA STATE UNIVERSITY

December 2011

ABSTRACT

Great advances have been made in the construction of photovoltaic (PV) cells and modules, but array level management remains much the same as it has been in previous decades. Conventionally, the PV array is connected in a fixed topology which is not always appropriate in the presence of faults in the array, and varying weather conditions. With the introduction of smarter inverters and solar modules, the data obtained from the photovoltaic array can be used to dynamically modify the array topology and improve the array power output. This is beneficial especially when module mismatches such as shading, soiling and aging occur in the photovoltaic array.

This research focuses on the topology optimization of PV arrays under shading conditions using measurements obtained from a PV array set-up. A scheme known as topology reconfiguration method is proposed to find the optimal array topology for a given weather condition and faulty module information. Various topologies such as the series-parallel (SP), the total cross-tied (TCT), the bridge link (BL) and their bypassed versions are considered. The topology reconfiguration method compares the efficiencies of the topologies, evaluates the percentage gain in the generated power that would be obtained by reconfiguration of the array and other factors to find the optimal topology. This method is employed for various possible shading patterns to predict the best topology. The results demonstrate the benefit of having an electrically reconfigurable array topology. The effects of irradiance and shading on the array performance are also studied. The simulations are carried out using a SPICE simulator. The simulation results are validated with the experimental data provided by the PACECO Company.

ACKNOWLEDGEMENTS

I would like to thank Dr. Cihan Tepedelenlioglu and Dr. Andreas Spanias for being my ideal advisors. Their help has been instrumental in keeping me motivated throughout my research. I am thankful to them for giving me an opportunity to work for the 'Statistical data processing of PACECO PV array monitors and GUI development' project. I am also thankful to the PACECO company for providing the photovoltaic array experimental data to carry out the research. Special thanks to Ted Yeider and Toru Takehara for their support. I am also grateful to Dr. Junshan Zhang for agreeing to serve on my dissertation committee.

I would also like to thank Ms. Darleen Mandt and Ms. Esther Korner for helping me with paperwork at all the different stages of my graduate studies.

I have received lot of assistance from my colleagues and friends in the Signal Processing and Communication research groups. Special thanks to my colleagues Venkatachalam Krishnan and Henry Braun for giving valuable suggestions and feedback to my research. I am also thankful to Lakshminarayan Ravichandran and Mahesh Banavar for providing assistance in times of help.

TABLE OF CONTENTS

LIST OF TABLES

Table Page

LIST OF FIGURES

Chapter 1

INTRODUCTION

This chapter discusses the motivation behind the topic of research, the objective and the existing work in the field of interest.

1.1 Motivation

Over the recent years, there has been an increased ecological awareness, pushing the development of renewable energies. The detrimental effects caused by fossil fuel consumption have lead to the acceptance of sustainability and the use of renewable energy sources have become a focus of interest. Among the renewable energies, photovoltaic (PV) energy is a compelling resource for power generation. It has environmental benefits: PV modules do not produce greenhouse gases while in operation and negligible amount during manufacturing. The modular nature of PV allows systems to be employed in various ranges of sizes. This allows short construction periods reducing technical and financial risks related to testing, pre-commercial deployment and commercial utilization. There are no complicated moving parts associated with the PV power generation. This results in a very low operating cost and maintenance. Also it is freely available and abundant in nature.

In spite of the several advantages, PV technology faces various barriers which prevent its wide deployment. The major barrier is the cost. The average levelized cost of energy (LCOE) for PV electricity was $211/MWh, while the LCOE of coal was only $95/MWh in the United States in year 2010 [2]. PV has overcome the cost problem with conventional energy only for special cases such as very remote locations where fuel shipping costs are extremely high. The other barrier with PV power generation is its dependence on the weather and with no effective method of storing energy, resulting in stability and reliability problems for the electrical grid. These issues suggest that any

technology that would lower the cost, improve reliability will increase the deployment of PV power generation.

PV modules are connected in series and parallel to form a photovoltaic array. The output of the array is affected by several factors such as solar irradiance, module rating, operating temperature, soiling, variation in the solar spectrum and angle of incidence [3]. The measurement of the array performance is associated with the study of these factors [4–6]. The efficiency of operation of a solar array depends not just on the weather conditions but also on the array topology [7, 8]. Conventionally, fixed PV array topology is determined taking into consideration the weather condition for the entire year. Therefore the fixed topology might not be an optimal configuration for a given weather condition. Also when the array consists of faulty (due to shading/ soiling) modules, the entire string current drops to the current generated by the under-performing module, resulting in a significant loss in the array output power. The fixed topology would not be able to bypass the under-performing modules. This operates the array in a non-optimal way and drops its efficiency. In these situations, the array can be reconfigured to an optimal topology that accommodates the present weather conditions and reduce the effect of faulty modules on the array's efficiency.

With the introduction of smart monitoring devices in the PV sector, there is a wide amount of data collected and an opportunity to relate the provided information. This data include voltage and current of PV modules/ array, module temperature and weather information. These measurements can be used to analyze the array behavior and optimize its efficiency. For example, the weather information and module temperature can be used to predict the energy generated by the array, compare with the actual generated output and analyze the array behavior. This information can be used to predict the optimal array topology. The array can be reconfigured to the optimal topology and increase its efficiency.

1.2 Objective

The Figure 1.1 shows a block diagram that summarizes the vision for optimizing a utility scale PV array. The monitoring devices connected to every PV module collect the individual module measurements (current, voltage and temperature) continuously. The collected information is transmitted to the server which stores past and current measurements of panel and weather data. A central operator accesses the data and can take action and issue various control commands to the PV array and the inverters. The 'Intelligent Networked PV System Management' will be equipped with various state of the art algorithms for data mining and stochastic prediction that identify and track various important time-varying events and patterns. The algorithms operate on PV array measurements and also parametric models for the modules and arrays to detect and diagnose faults quickly and remotely. The output of fault detection algorithm is used to determine PV array topologies that optimize the overall efficiency of the array for different environmental conditions. The PV array topology can then be reconfigured using the switching matrix and carry the power from the panels to the inverter through a combiner box. Stochastic signal and data processing algorithms will be used to predict weather and cloud patterns that will be used to determine PV module switching. Our research focuses on the 'Connection topology reconfiguration' block, which is equipped with reconfiguration algorithms to predict the optimal array topology.

The objective of this research is to propose dynamic reconfiguration of the PV array topology to ensure effective power generation under any shade condition. The topology reconfiguration method is described to find the optimal topology for the PV array. This method is used to find the efficiencies of the existing topologies along with a new bypassed and reconfigured topology for various possible shading scenarios in the array. The reconfigured topology would take into account, the current weather conditions and module faults, resulting in an increase in the array's efficiency.

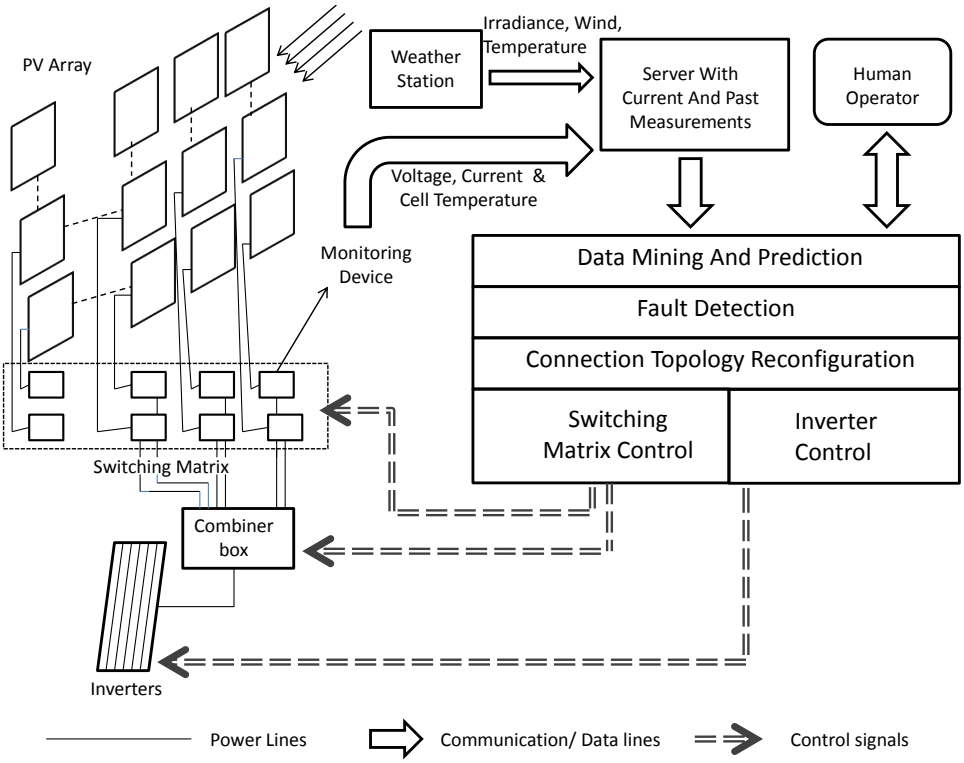

Figure 1.1: Intelligent Networked PV System Management.

1.3 Existing Methodologies

The major problems that cause the PV array to generate power less than the rated power are shading and improper selection of topology. To overcome the shading problem, several methods were put forward. The techniques and their associated drawbacks are discussed below:

Irradiance Equalization

The Irradiance Equalization method [9–11] is applied to PV arrays that are connected in total cross-tied (TCT) configuration (discussed in the Section 1.3). Depending on the irradiance received by the modules, they are relocated such that each row in the series string has similar irradiance. Since this method increases the power output of the array by equalizing the irradiance, it is known as 'Irradiance Equalization'. The relocation of the modules is achieved by employing a switching matrix.

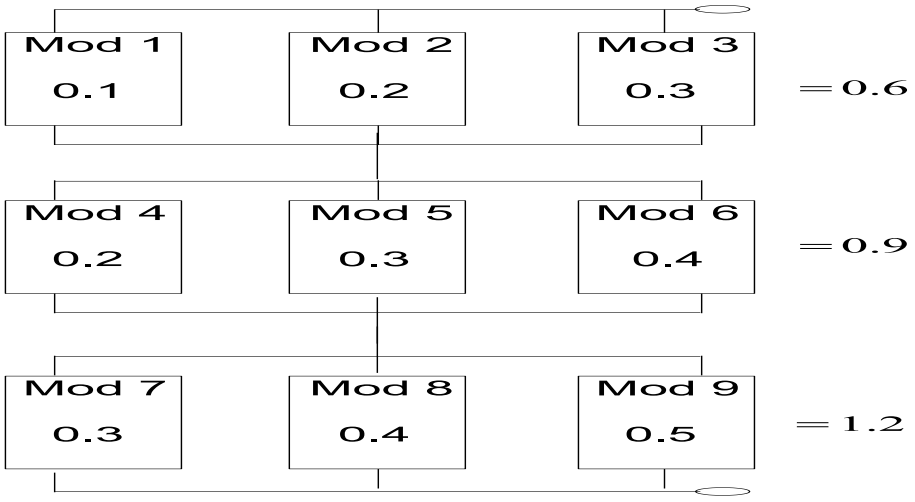

(a)

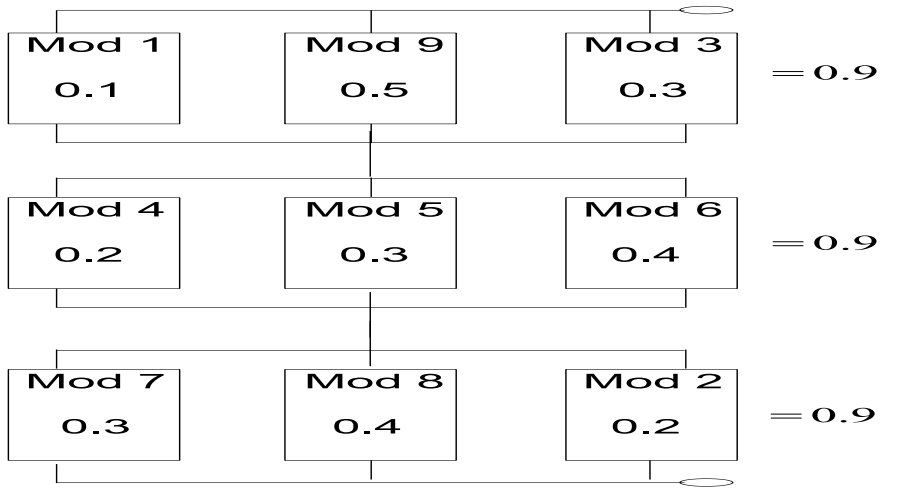

(b)

Figure 1.2: Demonstration of the Irradiance equalization method.

A shaded module when present in a string limits the current in the string to the current of the shaded module. By connecting PV modules with similar operating characteristics in a string would then increase the overall power output. The concept of irradiance equalization as demonstrated by [9] is shown in the Figure 1.2. The PV array consists of 9 modules connected in the TCT configuration. Each row in the Figure

consists of 3 modules connected in parallel and can together be considered as a single block module. The current generated by the block module is the sum of the currents of the individual modules. Three such block modules are connected in series. The effect of output current of each module normalized with repsect to the irradiance of 1000 W/m^2 (irradiance corresponding to standard test conditions) is calculated as the effective irradiance (dimensionles) using the diode equations described in [9].

The effective irradiance factor is the sum of the individual module effective irradiances. Figure 1.2 (a) shows block modules with unmatched effective irradiance factors. The switching matrix is then used to rearrange the electrical location of the modules 2 and 9 and the irradiance matched configuration is shown in the Figure 1.2 (b). The output for the configuration (b) is found to be higher. This is due to the fact that the current mismatch between the blocks is reduced before connecting them in series.

This method is applied on an array connected in a a fixed total cross-tied topology. Though there is reconfiguration within the topology, it might not be the optimal topology. Also, this method uses a switching matrix to relocate the modules. For larger arrays, the switching matrix becomes complicated and difficult to employ.

Adaptive Banking

The Adaptive banking method [12, 13] reconfigures the PV array to provide maximum power output under different shading conditions. Here the PV system has two parts- the fixed part and the adaptive part. The fixed part constitutes the PV array that is connected in total cross-tied (TCT) configuration. The adaptive part consists of a bank of individual PV modules. When the power output of the PV array (fixed part) goes down, the modules from the adaptive bank are connected in parallel to modules in the fixed part. This is accomplished by employing a switching matrix constructed using relays or electrical switches. The most illuminated solar module from the adaptive

bank is connected in parallel to the row of the fixed part that has the least power output (the most shaded row). In this manner all the modules from the adaptive bank are connected.

Consider an array of 16 modules connected in the total cross-tied (TCT) configuration as shown in the Figure 1.3 (a). Under normal operating conditions there is no need for any changes to the configuration. However, three of the modules in the array are currently severely shaded. The maximum current that can be generated by this array is now limited by the first row which has effectively only two healthy modules. This detrimental effect can be minimized to a certain extent by using the above discussed adaptive banking method. Here, the first three columns can be made the fixed part and the last column, the adaptive part. Each module in the adaptive part can be connected to any of the rows of the fixed part. This is accomplished by using the switching matrix constructed. With this arrangement, the severely mismatched condition of rows in the Figure 1.3 (a) can be rectified as shown in the Figure 1.3 (b). Here, two modules from the adaptive part of the array are added in parallel to the first row which has 2 modules shaded and one module is added to the second row which has one shaded module. Now, each row in the array has at least three non- bypassed modules, therefore the current is not restricted to two modules as in the previous case. If the mismatch is not severe, the most illuminated solar module from the adaptive bank is connected in parallel to the row of the fixed part that has the least power output (the most shaded row).

This method also employs the fixed total cross-tied topology and switching matrix to increase the efficiency of the array. Compared to the irradiance equalization method, it requires a switching matrix of smaller size as it relocates only the modules in adaptive bank rather than all the modules in the array. But it still uses a non-optimal fixed array topology and needs an additional set of modules allocated as the adaptive bank. The additional modules increase the cost of the system.

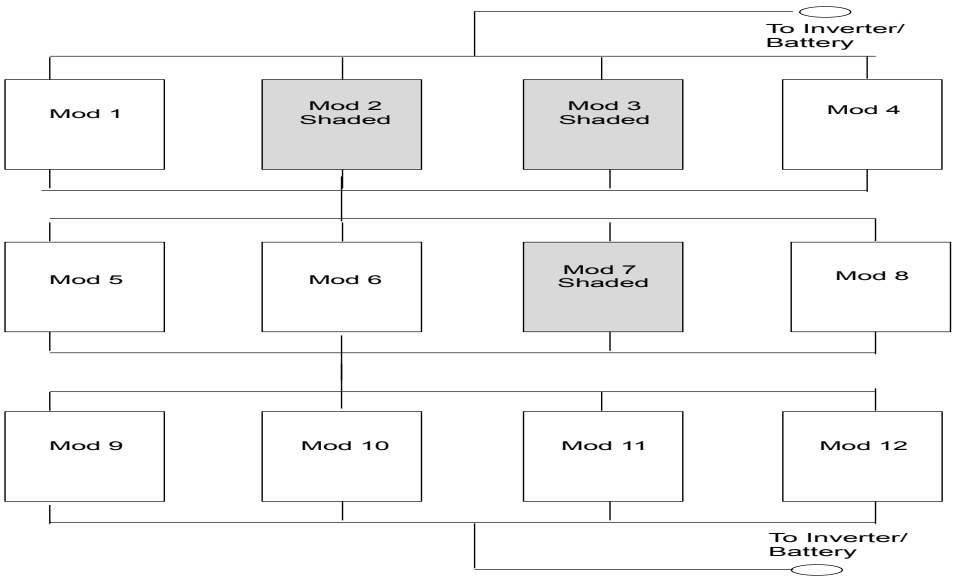

(a)

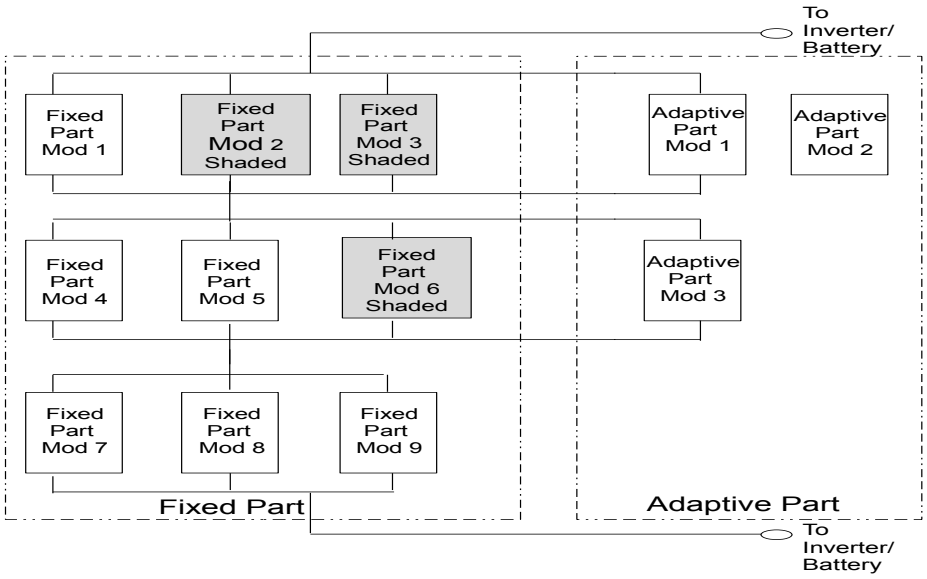

(b)

Figure 1.3: Demonstration of the Adaptive banking method.

Alternate Topologies

Alternate module interconnection schemes are suggested in [14] to overcome the mismatch losses, especially under shading conditions. Apart from the traditional series-

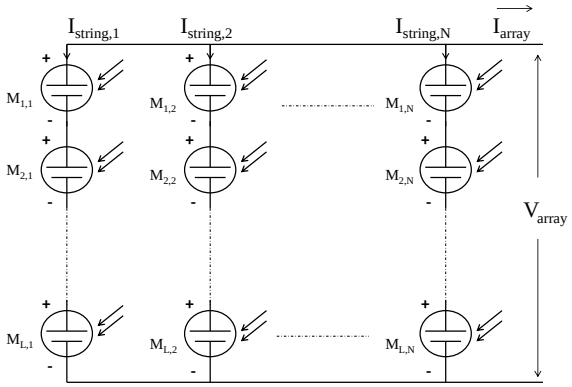

Figure 1.4: Photovoltaic modules connected in series-parallel (SP) configuration

parallel configuration (SP), alternate topologies such as bridge link (BL) and total cross-tied (TCT) configurations were analyzed in finding the topology with best performance. The topologies are shown in the Figures 1.4, 1.5 and 1.6. These alternate topologies help in the reduction of mismatch losses due to the additional redundancy in their configuration. The electrical behavior of the topologies is discussed in detail in the Section 2.5.

In [**?**], the TCT topology is shown to be the optimal topology for all possible shading patterns in an array consisting of four PV modules. It is experimentally shown in [15] that in an array with two shaded modules, changing the traditional series-parallel configuration to bridge link (BL) and total cross-tied (TCT) configurations resulted in a 4 % increase in the array power under shading conditions. Cross-tied topologies such as TCT and BL are shown to be more tolerant to mismatch losses caused due to aging and manufacturing process tolerances in [16, 17].

It is shown experimentally that the cross tied topologies perform well for a two shaded modules case [15]. But it is not guaranteed that the cross tied topologies alone would outperform all the existing topologies for any number of shaded modules (or any shading pattern) in the array.

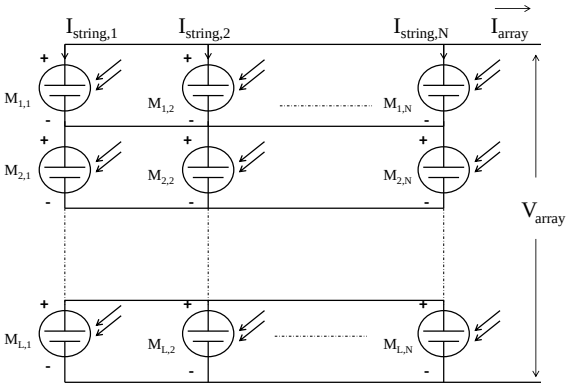

Figure 1.5: Photovoltaic modules connected in total cross-tied (TCT) configuration

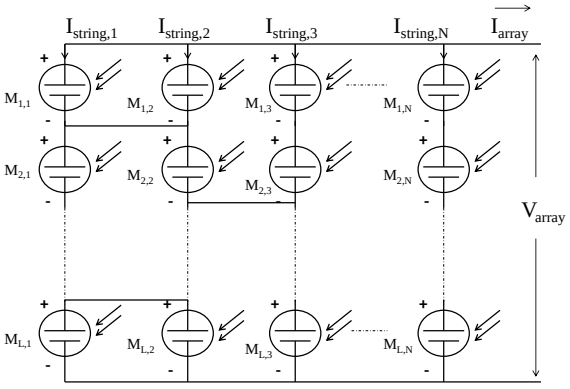

Figure 1.6: Photovoltaic modules connected in bridge link (BL) configuration

This research proposes dynamic reconfiguration of the array topology under shading to extract the maximum yield from the array. The topology reconfiguration method is used to find the optimal topology for given weather conditions and faulty module information. The efficiencies of the existing topologies along with a new by-passed and reconfigured topology are analyzed for various shading patterns.

1.4 Summary of Contributions

The contributions of this research can be summarized as follows:

- A topology reconfiguration method to predict the optimal topology for a PV array

consisting of shaded modules

- Simulation results implementing the topology reconfiguration method for various possible shading patterns
- Study of the effect of irradiance on the performance of array topologies
- Analysis of the behavior of array topologies with respect to shading phenomenon

1.5 Organization of the Book

The rest of this document is organized as follows. The physics of photovoltaic modules and arrays, design of array configuration and topologies used in practice are described in Chapter 2. The performance models used to predict array behavior are also explained in Chapter 2. The types of faults and the topology reconfiguration method are discussed in Chapter 3. In Chapter 4, simulation results implementing the topology reconfiguration method for various shading patterns are presented. The effect of irradiance and shading on the array performance is also studied. Chapter 5 presents the conclusions and future work.

Chapter 2

OVERVIEW OF PHOTOVOLTAICS

This chapter gives an outline of the topology reconfiguration system and discusses the physics behind the operation of a PV array. The various topologies that are employed in practice and their electrical behavior is presented. The models that can be used to predict the electrical characteristics of a PV module are explained.

2.1 Operation of a PV Module

The photovoltaic cell is the fundamental power conversion unit of a PV system [18] and is the component that produces electricity from solar energy. Although a single cell is capable of generating significant current, it operates at an insufficient voltage for typical applications. To obtain a higher voltage, cells are connected in series and encapsulated into a PV module/ panel. These modules show similar electrical behavior to individual cells. Similarly, modules are connected in series and parallel to form a photovoltaic array. The arrays generate direct current (DC) power which is converted to alternating current (AC) power using inverters.

The photovoltaic cell operation is based on the ability of a semiconductor to convert sunlight into electricity through the photovoltaic effect [18]. When sunlight is incident on the solar cell, the photons can either be reflected, absorbed or passed through it. Only the absorbed photons contribute to the generation of electricity. For a photon to be absorbed, its energy must be greater than the band gap of the solar cell, which is the difference between the energy levels of the valence band and conduction band in the cell. The absorbed photons generate pairs of mobile charged carriers (electrons and holes) which are then separated by the device structure (such as a p-n junction) and produce electrical current. A variety of materials facilitate the photovoltaic effect. In practice, semiconductor materials in the form of p-n junctions are mostly used to manufacture solar cells. To understand the operation of a solar cell, it is

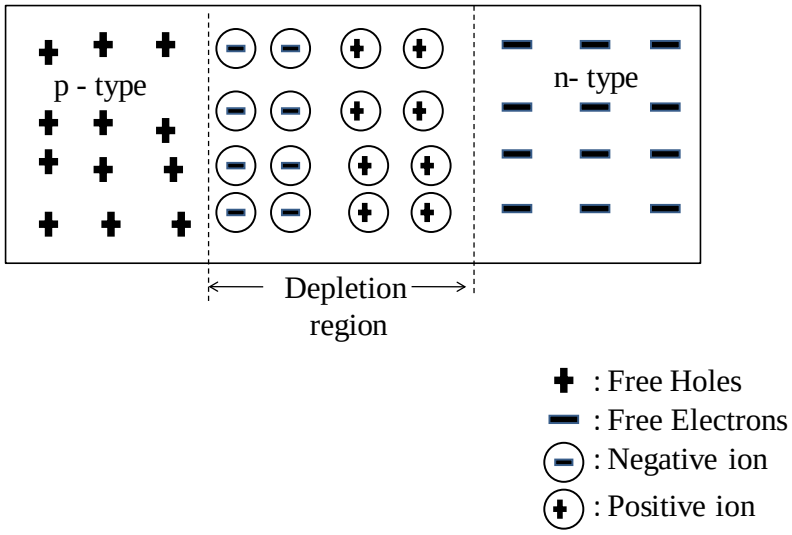

Figure 2.1: The p-n junction barrier formation

essential to know the functioning of p-n junctions.

Consider a p-n junction in a semiconductor. There is an electron surplus in the n-type semiconductor and a hole surplus in the p-type semiconductor. At the junction of the two semiconductors, the electrons from the n region near the interface diffuse into the p side. This leaves behind a layer of positively charged ions in the n region. In a similar fashion, holes diffuse in the opposite direction leaving behind a layer of negatively charged ions in the p region. The resulting junction region is devoid of mobile charge carriers. The positively and negatively charged ions (dopant atoms) present in the junction region result in a potential barrier which restricts any further flow of electrons and holes (as shown in the Figure 2.1). This potential barrier is known as the depletion region. The resultant electric field in the junction pulls electrons and holes in opposite directions [18]. Therefore current flow through the junction requires a voltage bias.

When an external bias is applied to the junction (Figure 2.2), for instance apply a negative voltage to the n-type material and a positive voltage to the p-type material. The negative potential on the n-type material repels electrons in the n-type material

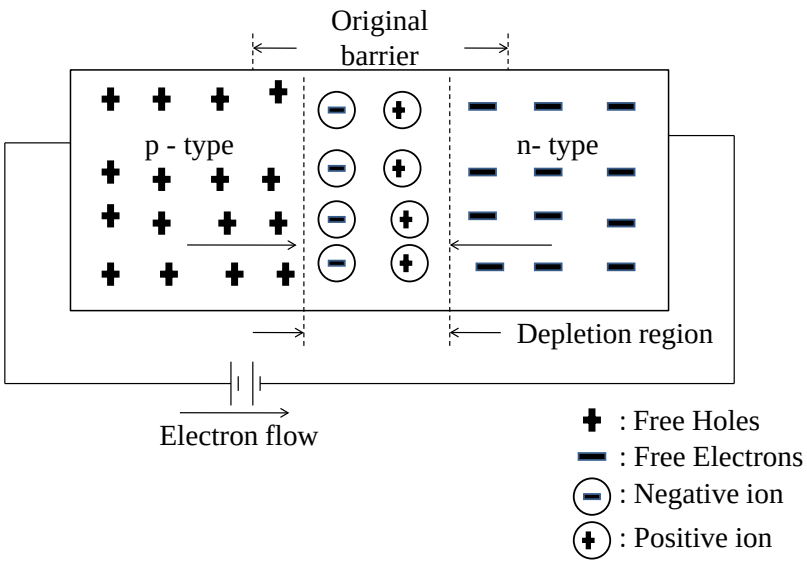

Figure 2.2: Forward biased p-n junction

and drives them towards the junction. Similarly the positive potential on the p-type material drives the holes towards the junction [19]. This reduces the height of the potential barrier. Consequently, there is a free motion of charges across the junction resulting in a dramatic increase in the current through the p-n junction. This is known as the *forward bias* situation.

When *reverse biased*, the p-type material is made negative with respect to the n-type material (Figure 2.3). Then the electrons in the n-type material are drawn towards the positive terminal and holes in the p-type material towards the negative terminal. Therefore, the majority charge carriers are pulled away from the junction. This results in an increase of the number of positively and negatively charged ions (dopant atoms), widening the depletion region [20]. Thus a continuous motion of charges is not established because of the high resistance of the junction [19] and the junction is said to be reverse biased. However the junction appears to be forward biased and provides low resistance to the minority carriers (electrons in p-type and holes in n-type regions). These minority carriers result in a minority current flow. This current known as the reverse saturation current (I_0), is much smaller in magnitude compared to the current generated

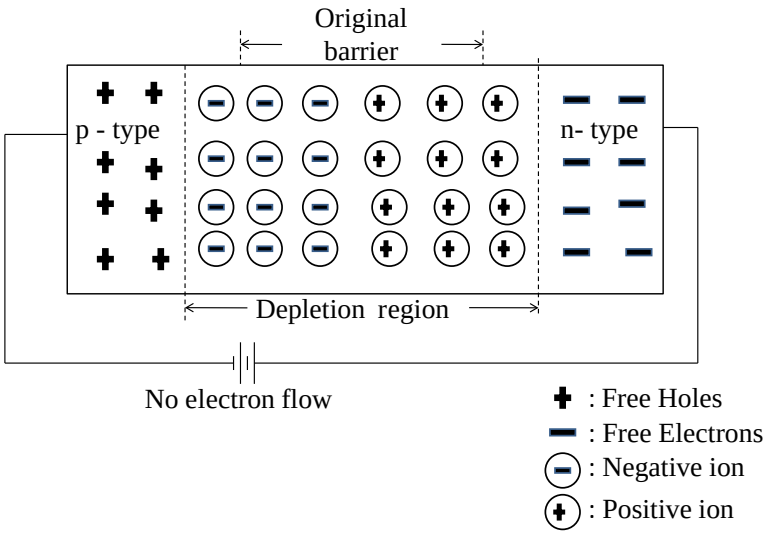

Figure 2.3: Reverse biased p-n junction

under forward bias. In the presence of an external source of energy such as light, heat etc., the electron hole pairs generate minority carriers which contribute significantly to current flow across the junction.

The I-V characteristic of a p-n junction diode is given by the Shockley equation [18]

$$I_{\mathrm{D}} = I_0 \left[\exp\left(\frac{qV_{\mathrm{D}}}{nkT_{\mathrm{cell}}} \right) - 1 \right], \tag{2.1}$$

where I_{D} is the current generated by the diode, V_{D} is the voltage across the diode, I_0 is the reverse saturation current of the diode (usually in the order of 10^{-10}A), q=1.602x10^{-19}Coulombs is the electron charge, T_{cell} is the cell temperature in Kelvin, n is the diode ideality factor (dimensionless) and k=1.38x10^{-23}J/K is the Boltzmann constant.

A p-n junction can be made to operate as a photovoltaic cell [19] (Figure 2.5). The p-n junction responds to the incident light photons and generates electric current. The influence of arriving photon energy produces a minority current effect [19]. These photons generate free electron-hole carriers which get attracted towards the junction. The electron and hole charges travel in opposite directions and set the direction of the

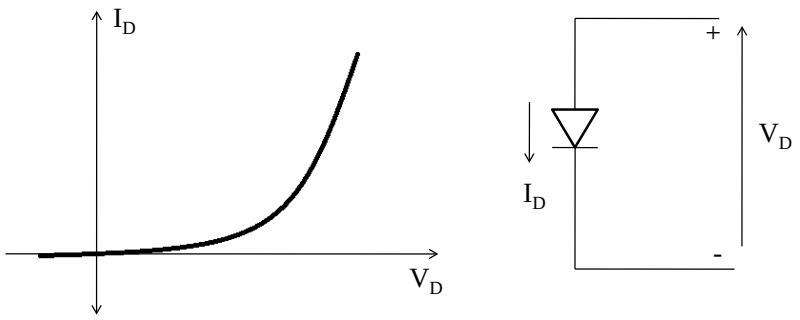

Figure 2.4: The diode I-V characteristic

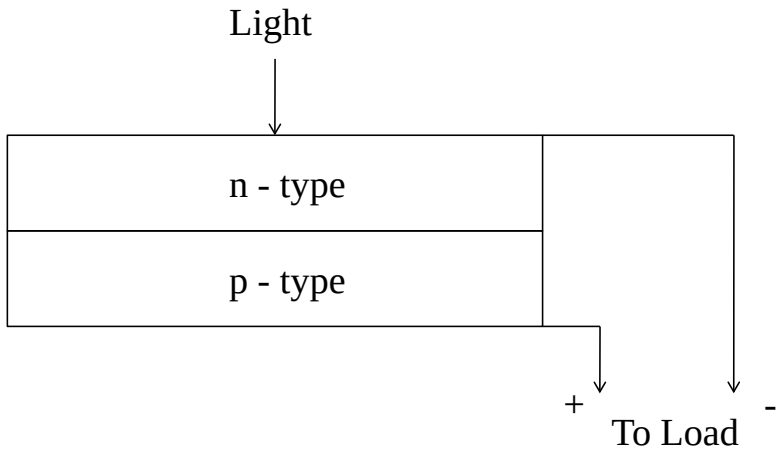

Figure 2.5: The photovoltaic cell connection

photovoltaic current as shown in the Figure 2.6 [19]. The electron flow in the circuit (shown in Figure 2.6) is from n-type silicon to p-type silicon [19]. The generated current varies with the light intensity.

The sign convention used for current and voltage in photovoltaics is such that the photocurrent is always positive. As shown in Figure 2.7, the light generated current, also known as photocurrent, is represented as I_{L}, the diode current as I_{D}, the net current and terminal voltage of solar cell as I_{cell} and V_{cell} respectively. The net current I_{cell} available from the solar cell is given as

$$I_{\mathrm{cell}} = I_{\mathrm{L}} - I_{\mathrm{D}}. \tag{2.2}$$

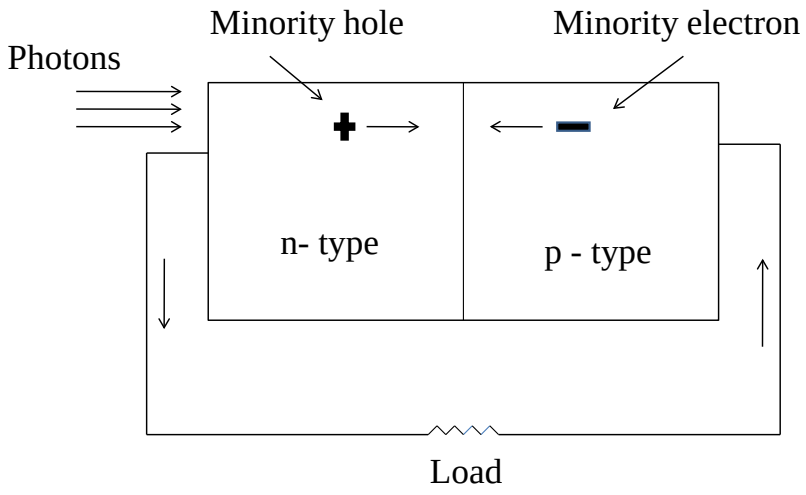

Figure 2.6: Operation of photovoltaic cell

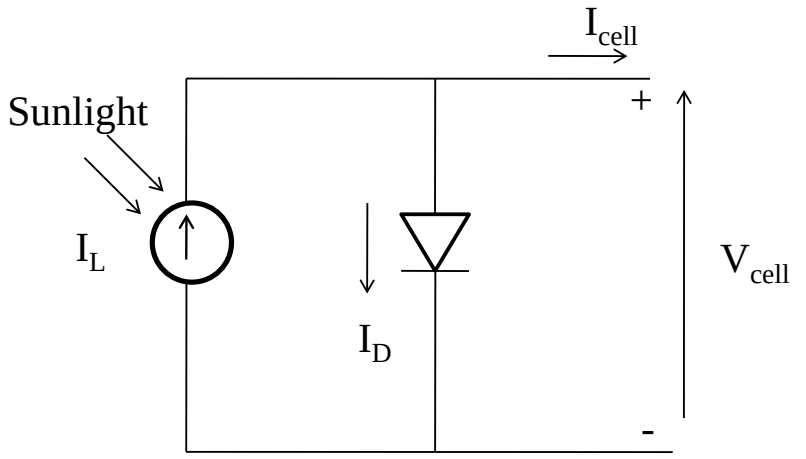

Figure 2.7: Equivalent circuit of an ideal photovoltaic cell

Substituting I_{D} from equation (2.1) into equation (2.2) [21],

$$I_{\mathrm{cell}} = I_{\mathrm{L}} - I_0 \left[\exp\left(\frac{qV_{\mathrm{cell}}}{nkT} \right) - 1 \right]. \tag{2.3}$$

Light generated current I_{L} increases linearly with solar irradiation. The smaller the diode current I_{D}, the more current is delivered by the solar cell. The ideality factor n of a diode is a measure of how closely the diode follows the ideal diode equation [21, 22]. Typically it takes values in between 1 and 3 [21]. The value $n = 1$ represents the

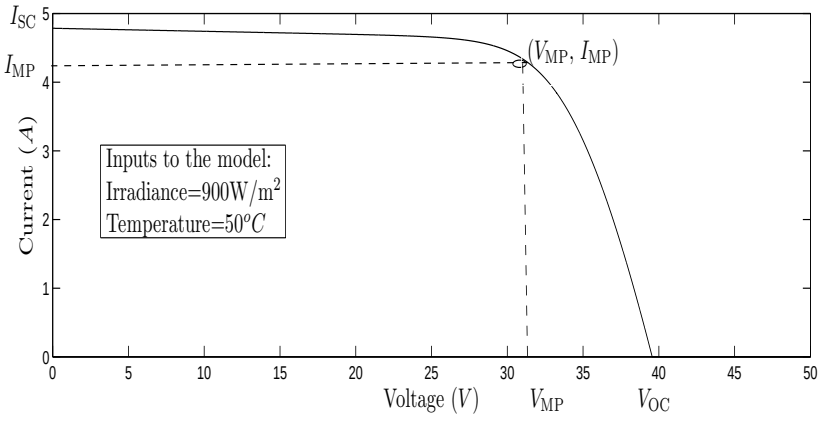

Figure 2.8: I-V characteristic of a photovoltaic module

ideal behavior of diode, while values $n>1$ correspond to non-ideal behavior leading to degradation in the cell efficiency [23]. The ideality factor value depends on irradiance, temperature and the type of recombination of charge carriers present in valence band and conduction band of the p-n junction diode [24].

2.2 Electrical Parameters of a Photovoltaic Cell

An example of the current-voltage (I-V) curve of a photovoltaic module is shown in Figure 2.8. The curve is obtained by using the five parameter model, discussed in Section 2.6 for a Sharp NT-175U1 photovoltaic module at an irradiance of 900 W/m^2 and module temperature of 50°C. The Sharp Nt-175U1 is used for all the simulations in this book. Unless otherwise mentioned, the irradiance and module temperature correspond to 900 W/m^2 and temperature of 50°C.

The parameters that determine the photovoltaic module's I-V characteristics are:

1. Short circuit current (I_{SC}): The largest current that a photovoltaic cell can generate is known as the short circuit current I_{SC}. It is the current generated by the photovoltaic cell when its voltage is zero (also shown in Figure 2.8). Ideally, when there are no resistive losses, the current generated by the solar cell is equal

to the short circuit current. For example, the short circuit current I_{SC} obtained from Figure 2.8 is 4.784 A.

2. Open circuit voltage (V_{OC}): The maximum voltage that can be generated across a photovoltaic cell is known as the open-circuit voltage V_{OC}. It corresponds to the condition when the net current through the photovoltaic cell is zero (refer Figure 2.8). Substituting $I = 0$ in equation (2.3) gives

$$V_{OC} = \frac{nkT}{q} \ln\left(\frac{I_L}{I_0} + 1\right). \tag{2.4}$$

This equation shows that the light intensity has a logarithmic effect on V_{OC}. Both light generated current I_L and dark saturation current I_0 depend on the structure of the device, but I_0 can vary by many orders of magnitude depending on the device geometry and processing [18]. Hence it is the value of I_0 that determines the open circuit voltage in practical devices. It can be observed from Figure 2.8 that power is generated only when the voltage is in between 0 and V_{OC}. For voltages outside this range, the device consumes power, instead of supplying it. The open-circuit voltage V_{OC} is obtained as 39.56 V from Figure 2.8.

3. Maximum power point power (P_{MP}): The maximum power P_{MP} produced by the solar cell is reached at a point on the I-V characteristic where the product IV is maximum [18]. This current and voltage are known as the maximum power current I_{MP} and maximum power voltage V_{MP} respectively. Therefore

$$P_{MP} = V_{MP} I_{MP}. \tag{2.5}$$

From Figure 2.8, V_{MP}, I_{MP}, and P_{MP} are obtained as 31.43 V, 4.33 A, and 136.09 W respectively.

4. Efficiency (η): The Efficiency (η) of a solar cell is defined as the ratio of the output energy of the solar cell to the input energy from the sun [21]. It is the

fraction of incident solar power that can be converted into electricity.

$$\eta = \frac{V_{OC} I_{SC} F}{P_{incident}}, \tag{2.6}$$

where $P_{incident}$ is the incident solar power and F is the fill factor of a solar cell. The fill factor is defined as the ratio of the maximum power generated by the solar cell to the product of I_{SC} and V_{OC} [21].

$$F = \frac{V_{MP} I_{MP}}{V_{OC} I_{SC}}. \tag{2.7}$$

Substituting for the fill factor in equation (2.6),

$$\eta = \frac{V_{MP} I_{MP}}{P_{incident}} = \frac{P_{MP}}{P_{incident}}. \tag{2.8}$$

Therefore efficiency is the ratio of the maximum power generated by the solar cell to the power incident on the solar cell.

Resistive Losses in a Solar Cell

Characteristic resistance (R_{ch}) of a solar cell is defined as the resistance of the solar cell at its maximum power point. If the resistance of the load (connected to the solar cell) is equal to the characteristic resistance, then solar cell operates at its maximum power point and delivers maximum power to the load. The characteristic resistance is given as

$$R_{ch} = \frac{V_{MP}}{I_{MP}}. \tag{2.9}$$

It is also approximated as [21],

$$R_{ch} = \frac{V_{OC}}{I_{SC}}. \tag{2.10}$$

The characteristic resistance is shown in Figure 2.9. Some of the power generated by the solar cell is dissipated through the *parasitic* resistances. These resistive effects are electrically equivalent to resistance in series R_s and resistance in parallel R_{sh} as shown in the Figure 2.10 [21]. The key impact of parasitic resistances is to reduce the fill

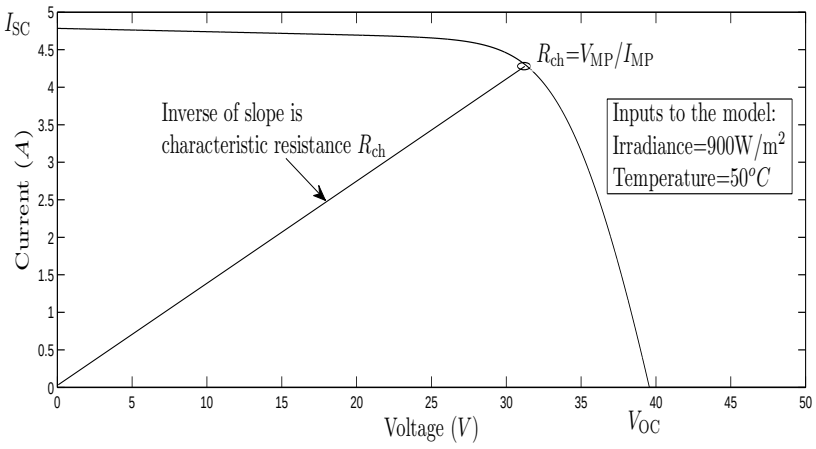

Figure 2.9: I-V curve obtained from five parameter model at an irradiance of 900 W/m^2 and temperature of 50^oC

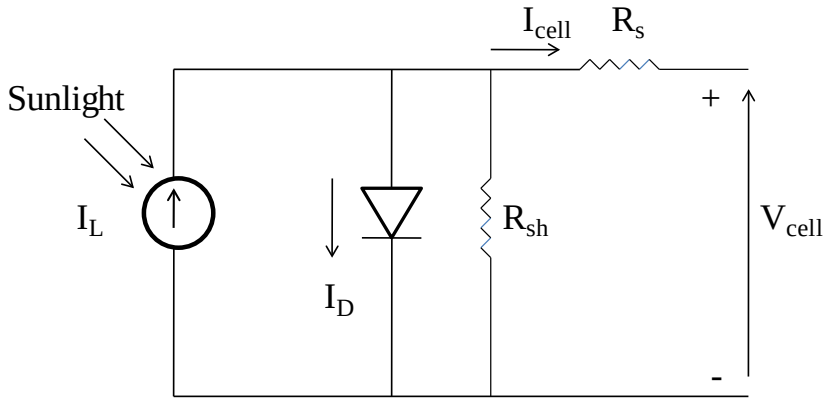

Figure 2.10: Parasitic series and shunt resistances in the equivalent circuit of a solar cell

factor. In the presence of these resistances, the current generated by the solar cell is given by [21]

$$I_{\text{cell}} = I_{\text{L}} - I_0 \exp\left[\frac{q\left(V_{\text{cell}} + I_{\text{cell}}R_{\text{s}}\right)}{nkT}\right] - \frac{V_{\text{cell}} + I_{\text{cell}}R_{\text{s}}}{R_{\text{sh}}}. \tag{2.11}$$

The series resistance R_{s} is the resistance offered by the material of the solar cell to the current flow [22]. Its main effect is to reduce the fill factor and therefore the efficiency of cell. Excessively high values of R_{s} may also reduce the short circuit current [21]. On the other hand, the shunt resistance R_{sh} is a result of the manufacturing defects

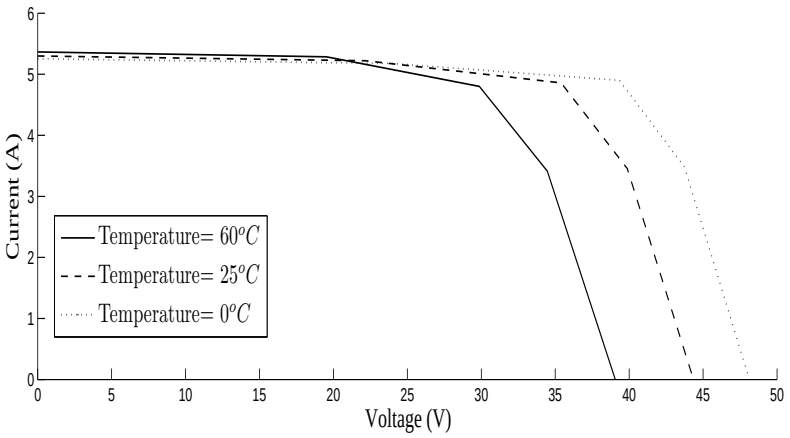

Figure 2.11: Temperature dependence on the I-V characteristic of a solar cell

in the solar cell. Low shunt resistances provide an alternate current path for the light generated current, thereby reducing the terminal voltage of the solar cell. This effect is more pronounced at lower irradiances, since there will be less light generated current [21]. For an efficient solar cell, R_s should be as small and R_{sh} as large as possible.

2.3 Effect of Temperature and Irradiance

The power output of solar cells is significantly affected by variations in the temperature and irradiance. This section describes their impact on the characteristics of the solar cell.

Temperature

The most significant effect of temperature is on the cell terminal voltage V_{cell}. It decreases with increase in temperature, i.e it has a negative temperature coefficient. The impact of temperature on current is less pronounced. Figure 2.11 shows the effect of temperature on the I-V characteristic at a constant irradiance of 1000 W/m^2.

Irradiance

The I-V characteristics of solar cell under different levels of illumination are shown in Figure 2.12. It is observed that the light generated current I_L is directly proportional to the irradiance. Therefore the short circuit current is directly proportional to the

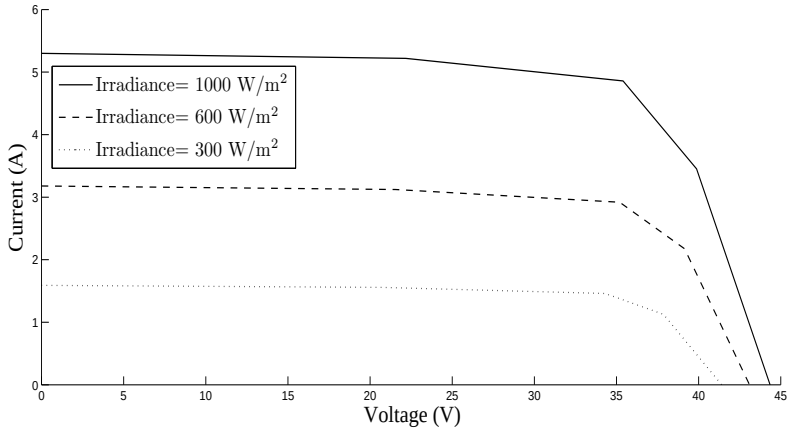

Figure 2.12: Irradiance dependence on the I-V characteristic of a solar cell

irradiance. The voltage variation is much smaller due to its logarithmic dependence on the irradiance and it is usually neglected in practical applications [19]. Figure 2.12 shows the effect of irradiance on the I-V characteristic at a constant temperature of 25^oC.

2.4 Design of Feasible Configurations

The design methodologies for PV arrays are specified in [25]. The number of modules in a series string is limited by the operating range of the inverter. The maximum voltage that can be generated by the array should not exceed the maximum input voltage to the inverter. As the module voltage increases at lower temperature, the open circuit voltage of the inverter should not surpass the maximum operating voltage of the inverter on the coldest day of the year. The maximum number of modules $N_{\max}$, that can be connected in a string is given by

$$N_{\max} = \frac{V_1}{V_2}, \tag{2.12}$$

where, V_1 is the maximum input voltage of the inverter and V_2 is the open circuit voltage of a module at the lowest winter temperature of the year.

The minimum number of modules $N_{\min}$ that can be connected in a string is determined by the minimum input voltage requirement of the inverter and the maximum

temperature at which the modules need to operate. It is given as

$$N_{\min} = \frac{V_3}{V_4}, \tag{2.13}$$

where, V_3 is the minimum input voltage of the inverter at maximum power point (MPPT) and V_4 is the MPPT voltage of a module at the highest module temperature during the year. Other factors such as the efficiency of the inverter at different voltages can be considered to determine the exact number of modules in a string.

The limitation on the number of strings that can be connected in parallel is determined by the maximum input current to the inverter and the current carrying capacity of the wires used. The maximum number of strings in parallel N_{P} is given by

$$N_{\mathrm{P}} = \frac{I_1}{I_2}, \tag{2.14}$$

where, I_1 is the maximum current that can be input to the inverter, I_2 is the short circuit current at maximum irradiance for the given string.

National Electric Codes govern the tolerance levels for the current carrying wires used in the construction of the PV arrays. The codes require the wires used to be rated at at-least 156.25% of the maximum short circuit current they might expected to carry. This restrains the maximum number of strings that can be kept in parallel in addition to the restriction imposed by the equation (2.14).

2.5 Topologies in Practice

Photovoltaic cells are electrically combined together to form a photovoltaic module. The schematic symbol for a photovoltaic cell or module is shown in Figure 2.13. Photovoltaic modules are interconnected in series-parallel combinations to form a photovoltaic array as shown in Figure 1.4. The limits on the number of modules to connect in series and parallel is discussed in the Section 2.4. This section discusses the electrical characteristics of a photovoltaic array under ideal conditions.

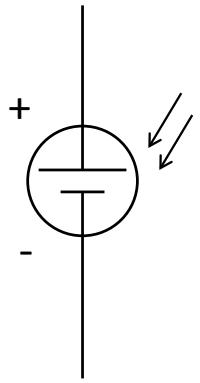

Figure 2.13: Photovoltaic module symbol

In the Figure 1.4 the photovoltaic array consists of L modules connected in series to form a string and N such strings are connected in parallel. Each photovoltaic module is represented by $M_{i,j}$, where 'i' and 'j' represent the row number and column number respectively. The current and voltage of a module $M_{i,j}$ are represented by $I_{i,j}$ and $V_{i,j}$ respectively. The modules present in a string carry same amount of current and the string current equals the module current. The string voltage is the sum of the voltages of individual modules in the string. The string current and voltage are obtained as,

$$I_{\text{str},j} = I_{i,j} = I_{k,j} \text{ , } \forall \text{ i, k where j= 1, 2,.., N and} \tag{2.15}$$

$$V_{\text{str},j} = \sum_{i=1}^{L} V_{i,j} \text{ where j= 1, 2,.., N.} \tag{2.16}$$

When strings are connected in parallel to form an array, the array current equals the sum of the currents from each string. The array voltage is same as the voltage of any string voltage. The current and voltage of an array are obtained as,

$$I_{\text{arr}} = \sum_{j=1}^{N} I_{\text{str},j} \text{ and} \tag{2.17}$$

$$V_{\text{arr}} = V_{\text{str},j} = V_{\text{str},k} \text{ , } \forall \text{ j, k.} \tag{2.18}$$

The power of the array is obtained as

$$\begin{aligned} P_{\text{arr}} &= V_{\text{arr}} I_{\text{arr}} \\ &= (LV_{1,1})(NI_{1,1}) \\ &= LNP_{1,1}. \end{aligned}$$

where $P_{1,1}$ represents power of the module $M_{1,1}$. Therefore under ideal conditions, the array power output is equal to the sum of the powers of individual modules.

Apart from the series-parallel combination, the modules can also be connected in a cross-tied manner in which additional connections are introduced between the modules. There are two kinds of cross-tied topologies: the total cross-tied (TCT) topology and the bridge link (BL) topology. In the total cross-tied topology as shown in Figure 1.5, each of the photovoltaic modules is connected in series and parallel with the others [14]. The bridge link topology shown in Figure 1.6, consists of half of the interconnections when compared to the total cross-tied topology [14]. Ideally when there are no wiring losses and module mismatches, all the modules behave identically and the performance (the generated array power) is the same for the series-parallel and cross-tied topologies. When there are electrical mismatches, one of the topologies outperforms the others.

2.6 Existing Models for PV Cell/ Module

Manufacturers of photovoltaic modules provide electrical parameters only at standard test conditions (irradiance = 1000 W/m^2 and $T_{\text{cell}} = 25^oC$) [26]. They provide the short circuit current I_{SC}, the open circuit voltage V_{OC}, the voltage at maximum power point V_{MP}, the current at maximum power point I_{MP} and the temperature coefficients at open circuit voltage and short circuit current [26]. The nominal operating cell temperature determined at an irradiance of 800 W/m^2 and an ambient temperature of 20^oC is also specified [27]. However, PV modules operate over a large range of conditions and the information provided by manufacturers is not sufficient to determine their overall

performance. This makes necessary the need for an accurate tool to determine the module behavior. Photovoltaic performance models are therefore built to predict the performance of a photovoltaic module at any operating condition. A PV model finds the I-V characteristic of a PV module as a function of temperature, incoming solar irradiation (direct and diffuse), angle of incidence and the spectrum of sunlight. Angle of incidence (degrees) is the angle between a line perpendicular (normal) to the module surface and the beam component of sunlight [6]. Models are also used to monitor the actual versus predicted module's performance and detect problems that affect the module's efficiency [6].

In this section models that determine the module's behavior on the DC side of the inverter are discussed. Sandia model and five parameter model are some of the accurate models widely used to predict the module's performance on the DC side of the inverter. Then the dependency of the models on weather data is explained.

The Sandia Model

Sandia National Laboratories developed a photovoltaic module and array performance model [6]. It uses a database of empirically derived parameters developed by testing modules from a variety of manufacturers to predict photovoltaic module/array performance [28].

The Sandia model is based on a set of equations that describe the electrical performance of the photovoltaic modules. These equations can be used for any series or parallel combination of modules in an array. They calculate the four points necessary to define the I-V curve of the photovoltaic module/array. These are the short circuit current (I_{SC}), the open circuit voltage (V_{OC}), the voltage at maximum power point (V_{MP}) and the current at maximum power point (I_{MP}). Two other currents are calculated at intermediate values for modeling the curve shape. These are defined at a voltage equal to half of the open circuit voltage and at a voltage midway between the voltage at maximum power point and open circuit voltage. All these parameters are found by a curve

fitting process of the coefficients obtained from testing of the modules. Empirical coefficients are also developed to determine parameters that are temperature dependent, effects of air mass and angle of incidence on the short circuit current and type of mounting (whether rack mounted or building integrated PV systems) [28]. This model also determines the effective irradiance, defined as the fraction of the total irradiance incident on the modules to which the cells actually respond (dimensionless or 'suns') [6]. Effective irradiance is used in the calculation of model's parameters.

The primary equations employed to find the I-V characteristics are given below [6]:

$$I_{\mathrm{SC}} = I_{\mathrm{SC0}} f_1(AM_{\mathrm{a}}) \frac{[E_{\mathrm{b}} f_2(AOI) + f_{\mathrm{d}} E_{\mathrm{diff}}]}{E_{\mathrm{o}}} \left[1 + \alpha_{I_{\mathrm{SC}}}(T_{\mathrm{c}} - T_{\mathrm{o}})\right], \tag{2.19}$$

$$V_{\mathrm{OC}} = V_{\mathrm{OC0}} + N_{\mathrm{s}} \delta(T_{\mathrm{c}}) \ln(E_{\mathrm{e}}) + \beta_{V_{\mathrm{OC}}} E_{\mathrm{e}}(T_{\mathrm{c}} - T_{\mathrm{o}}), \tag{2.20}$$

$$V_{\mathrm{MP}} = V_{\mathrm{MP0}} + C_2 N_{\mathrm{s}} \delta(T_{\mathrm{c}}) \ln(E_{\mathrm{e}}) + C_3 N_{\mathrm{s}} \left(\delta(T_{\mathrm{c}}) \ln(E_{\mathrm{e}}^2)\right)^2 \tag{2.21}$$

$$+ \beta_{V_{\mathrm{MP}}} E_{\mathrm{e}}(T_{\mathrm{c}} - T_{\mathrm{o}}), \tag{2.22}$$

where

$$E_{\mathrm{e}} = \frac{I_{\mathrm{SC}}}{I_{\mathrm{SC0}}\left[1 + \alpha_{I_{\mathrm{SC}}}(T_{\mathrm{c}} - T_{\mathrm{o}})\right]} \tag{2.23}$$

$$\delta(T_{\mathrm{c}}) = \frac{nk(T_{\mathrm{c}} + 273.15)}{q}. \tag{2.24}$$

The parameters introduced above are defined in Table 2.1 [6].

An I-V curve of the Sandia model, programmed in MATLAB is shown in the Figure 2.14. The program for Sandia model is provided in the Appendix.

The Sandia model is validated using experimental data from different geographic locations provided by the National Institute for Standards and Technology (NIST) [28]. The model can be used to predict output power within 1 percent of the

Parameter	**R**epresentation
N_s	Number of cells in series in a module's cell-string
N_p	Number of cell-strings in parallel in a module
T_c	Cell temperature inside module (^oC)
T_o	Reference cell temperature typically 25^oC
E_o	Reference solar irradiance typically 1000W/m^2
$\delta(T_c)$	Thermal voltage per cell at temperature T_c
E_b	Beam component of solar irradiance
E_{diff}	Diffuse component of solar irradiance
f_d	Fraction of diffuse irradiance used by module
AM_a	Absolute air mass (dimensionless)
AOI	Solar angle of incidence (degrees)
$f_1(AM_a)$, $f_2(AOI)$	Empirically determined polynomials
C_1, C_2, C_3 , C_4	Empirically determined coefficients

Table 2.1: Parameters of Sandia model

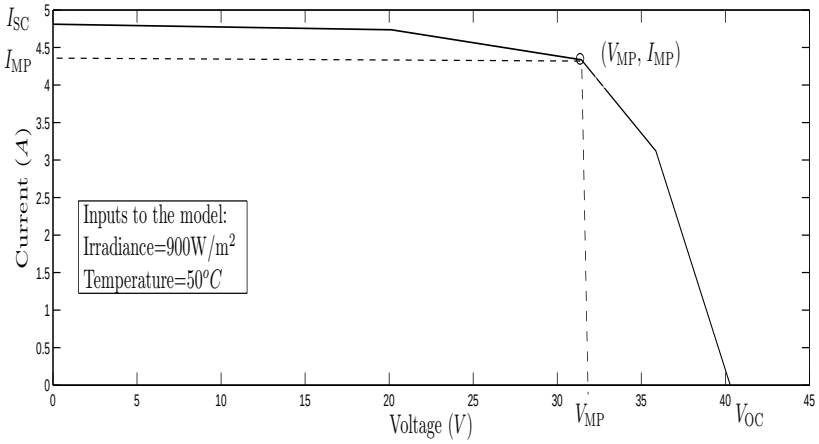

Figure 2.14: I-V curve obtained from Sandia model at an irradiance of 900W/m^2 and temperature of 50^oC

measured power and is considered to be the most accurate of all the available performance models [28]. However, it has limitations in that it requires several parameters that are not available from the manufacturer which necessitates additional testing of the modules.

The Five Parameter Model

The five parameter model developed at the Wisconsin Solar Energy laboratory, uses the well known single diode model shown in the Figure 2.10 to evaluate the performance

of PV modules. The five parameter model predicts the maximum power and I-V characteristics of a photovoltaic module at any operating condition. It utilizes only data provided by the manufacturer at standard test conditions. This model has five parameters: the light generated current I_{L}, the diode reverse saturation current I_0, the series resistance R_{s}, the shunt resistance R_{sh} and the modified ideality factor a (see Figure 2.10) [26]. The modified ideality factor in terms of ideality factor n is given as

$$a = \frac{N_{\mathrm{s}} n k T_{\mathrm{cell}}}{q}, \tag{2.25}$$

where N_{s} represents the number of cells in series.

From Figure 2.10, the current generated by the photovoltaic module (I_{mod}) is given as [27],

$$I_{\mathrm{mod}} = I_{\mathrm{L}} - I_0 \left[\exp\left(\frac{V_{\mathrm{mod}} + I_{\mathrm{mod}} R_{\mathrm{s}}}{a} \right) - 1 \right] - \frac{V_{\mathrm{mod}} + I_{\mathrm{mod}} R_{\mathrm{s}}}{R_{\mathrm{sh}}}, \tag{2.26}$$

where, V_{mod} is the terminal voltage of the module. The five parameter model is semi-empirical as it calculates parameters theoretically, from known relationships and equations derived from previous studies [28]. The model first calculates the reference parameters, i.e the parameters at standard test conditions, using the available manufacturer's data. These values are used to find the parameters at any operating condition. An easy to use application to determine the reference parameters was developed by the University of Wisconsin [29]. A sample I-V curve of the five parameter model implemented in MATLAB is shown in Figure 2.8. A MATLAB implementation of the five parameter model is provided in the Appendix.

Five parameter model is compared with Sandia model and experimental data provided by National Institute of Standards and Technology (NIST) in the following section.

Comparison of the Sandia and the Five Parameter Models

The experimental data provided by the National Institute of Standards and Technology (NIST) is used to examine the efficiency of the five parameter and Sandia models [26].

Irradiance (W/m^2)	Temperature (^oC)	Maximum power (W/m^2)		
		NIST	King	Five-parameter
1000.0	25.0	133.4	133.4	133.4
882.6	39.5	109.5	111.4	110.6
696.0	47.0	80.1	82.0	82.4
465.7	32.2	62.7	61.1	61.0
189.8	36.5	23.8	22.5	22.3

Table 2.2: Maximum power values from NIST measurements and the King and five-parameter models for the single-crystalline cell type [1]

Irradiance (W/m^2)	Temperature (^oC)	Maximum power (W/m^2)		
		NIST	King	Five-parameter
1000.0	25.0	125.8	125.8	125.8
882.6	39.5	106.8	109.3	105.6
696.0	47.0	77.4	79.1	78.1
465.7	32.2	56.6	56.9	55.8
189.8	36.5	21.2	18.5	20.6

Table 2.3: Maximum power values from NIST measurements and the King and five-parameter models for the poly-crystalline cell type [1]

Irradiance (W/m^2)	Temperature (^oC)	Maximum power (W/m^2)		
		NIST	King	Five-parameter
1000.0	25.0	104.0	104.0	104.0
882.6	39.5	83.7	87.3	85.5
696.0	47.0	59.9	62.3	62.3
465.7	32.2	40.8	43.2	44.3
189.8	36.5	14.4	15.7	16.3

Table 2.4: Maximum power values from NIST measurements and the King and five-parameter models for the silicon thin film cell type [1]

The models are compared for the four different cell technologies: single-crystalline, poly-crystalline, silicon thin film and triple-junction amorphous. The maximum power point values obtained from the models is compared with the NIST data and tabulated for each of the technologies as shown in the tables 2.2, 2.3, 2.4 and 2.5.

Irradiance (W/m^2)	Temperature (^oC)	Maximum power (W/m^2)		
		NIST	King	Five-parameter
1000.0	25.0	115.8	115.8	115.8
882.6	39.5	94.2	98.9	100.8
696.0	47.0	78.5	81.2	76.8
465.7	32.2	51.7	57.8	61.2
189.8	36.5	22.6	25.4	22.0

Table 2.5: Maximum power values from NIST measurements and the King and five-parameter models for the triple junction amorphous cell type [1]

It is observed that the Sandia model shows slightly better agreement with the data in contrast with the five parameter model. This is expected as the Sandia model requires many measurements over a wide range of conditions to determine the model parameters (as seen in the Section 2.6), whereas the five parameter model uses only the manufacturer's data to find the I-V characteristics. The predictions from the five parameter model could be better if I-V curves corresponding to two different irradiance values (one at lower irradiance and the other at higher irradiance) are provided instead of one [26]. It is also to be noted that there are uncertainties inherent in the experimental data.

Model Dependency on Weather Data

The reliability of a model output depends on the accuracy of the input weather data to a large extent. As the memory of the weather instrumentation is limited, there is a condition imposed on the sampling rate of the measurements. Typically two kinds of data reduction methods are used. The weather data is sampled at a low rate (known as under-sampling) or sampled at a high rate and then averaged in order to reduce the amount of data collected. The effect of these methods on the accuracy of a model was studied by Sandia National Laboratories using the Sandia model.

Sandia National Laboratories collected weather data approximately every three seconds for several days in late August to mid-September, 2008 [30]. The model output for this high resolution weather data is used to compare the model output with weather

data obtained from the two methods: under-sampling and averaging. From the comparisons, it is observed that the error rate increases as the sampling or averaging size becomes large. It is also evident from the results shown in [30] that under-sampling causes larger errors than sampling more frequently and averaging.

While using sample and average method, during the days of high variability in weather data, say irradiance for example, the high and low irradiances blend to medium irradiances. At medium irradiances, modules which show higher efficiencies over-predict energy generation while those with lower efficiencies under-predict energy generation. Therefore depending on the data variability of a site, a sampling or averaging rate may be selected such that measurements are expected not to exceed a given error threshold [30].

Chapter 3

TOPOLOGY RECONFIGURATION METHOD

This chapter discusses the various types of faults that occur in a PV array. It also describes the topology reconfiguration method that can be used to find the optimal array topology under shading conditions.

3.1 Overview of Types of Faults

An overview of module faults is presented to explain their effect on the module's performance. The array power of an ideal solar array is the sum of powers of individual modules. In this case, the calculation of array voltage and array current is fairly simple. However in practice, the available DC power from the array is substantially lower than the predicted levels. This is attributed to various kinds of module faults that occur in the solar array. Under faulty conditions such as shading and soiling, topology reconfiguration can be used to increase array's efficiency. This section discusses the major types of faults.

Module Mismatch

Photovoltaic modules have variable electrical characteristics inevitably caused by the variation in manufacturing processes. The optimal current and voltage can differ from module to module in an array at a given point in time. These variations result in reduction of the output power of the array, because of the constraints imposed by the array's electrical configuration. Module mismatches cause the modules operate at a suboptimal point on the current-voltage (I-V) curve, thereby reducing the array's output power. Though the manufacturing processes are improved, the module mismatches must be considered [31].

Module Soiling

Module soiling is the accumulation of dirt on the surface of a PV module. Researchers found that the effects of soiling are small (2.3% loss of power) for directly incident

light but become significant for larger angles: a loss of 8.1% was observed in a soiled module when light was incident from an angle of 56 degrees [32]. Bird droppings also cause a significant degrading effect due to their complete blockage of light over a small area. A soiled module causes a mismatch in the effective irradiance received by the module, reducing the performance of the array.

Shading

Shading is the phenomenon in which the surface of PV module is partially or totally blocked from sunlight. It is a very serious concern in PV arrays [33–35]. It causes significant reduction in the module's performance if not addressed in time. When a PV cell is shaded, its light-generated current decreases reducing the maximum power point current I_{MP} of the module. For a total shade, i.e, 100% shading results in I_{SC}=I_{MP}=0 and the PV module acts like a diode, consuming rather than producing current. This heats up the shaded module, producing a 'hot spot'. These hot spots can lead to module failure dramatically reducing the array efficiency.

When a shaded module is connected to unshaded modules in a series-parallel configuration, the current of the string consisting the shaded module is constrained to operate at the reduced current of the shaded module. This restricts the string current and hence the power available from the remaining unshaded modules. To avoid this, PV modules are equipped with bypass diodes. The bypass diodes provide alternate paths for the current and mitigate the effect of severe mismatches.

Ground Fault

A ground fault occurs when the PV module develops an unintentional path to ground. This results in a reduced output voltage and power, and can be fatal if the leakage currents run through a person. Ground fault circuit interrupters (GFCIs) can detect very small (6 mA) leakage currents and stop current flow within 200 ms. Although there are specific issues related to the detection of DC ground faults, GFCIs used in

PV arrays are fairly similar to the AC devices found in modern bathrooms. GFCIs are a mature technology and are mandated for all PV systems by the 2008 United States National Electric Code [36].

DC Arc Fault

Direct current (DC) arcing is a spark caused across air or any other dielectric. It occurs in two forms: series and parallel [37–39]. A series arc occurs when a connection breaks, leaving two conductors very near to each other. They can occur in junction boxes, at the cable connections between modules, and within modules. A parallel arc can occur when two conductors of different voltage are near each other. Arcs result in an inefficiency in the array operation, cause failure of bypass diodes [40] and can even cause fires.

The shading and soiling faults effectively result in a decrease in the amount of irradiance received by the module and reduces its output power. The effects caused by the reduction in the irradiance are addressed in this research.

3.2 Topology Reconfiguration Method

An ideal PV array connected in any topology performs identically. But when faults occur in the array, the performance of the topologies differs and the current array topology may not produce the maximum yield. In this section, a topology reconfiguration method is proposed to predict the optimal topology for a photovoltaic array consisting of shaded modules. This method assumes that the PV system is provided with an array reconfiguration facility. The topology reconfiguration method can be implemented in monitoring systems to predict the best suitable array configuration for a definite time period using the previous array's measurements. For the intelligent networked PV management shown in Figure 1.1, the topology reconfiguration method can be used in the 'connection topology reconfiguration' block to predict the optimal array configuration.

The topology reconfiguration method is described in the block diagram shown

in the Figure 3.1. The operation of the blocks is explained below.

Fault Detection Algorithm

The monitoring system provides the plane of array (POA) irradiance and the module level measurements: the maximum power point voltage (V_{MP}), maximum power point current (I_{MP}), module temperature and the aging information, which can be used to detect faults using the fault detection algorithms. In general, the faulty modules form a cluster in the I-V space, while the rest of the string in which the fault occurs forms another cluster, and the remaining unaffected modules in the string form a third cluster. One such state of the art algorithm to detect the shaded modules is explained in [41].

Reconfigurable Topologies

The feasible configurations of the array, i.e, the number of modules that can be connected in a string and the number of strings that can be connected in parallel are determined from the inverter specifications, wiring requirements and module specifications as explained in the Section 2.4. The feasible configuration can be connected in several topologies such as the series-parallel (SP), bridge link (BL) and total cross-tied (TCT), discussed in the Section 1.3 [15]. These topologies form the set of topologies to which the array can be configured to, known as the reconfigurable topologies.

The information from the fault detection algorithms is also used to find reconfigurable topology/ topologies. For example in the case of shading, the faulty modules can be bypassed based on the intensity of shading. A new topology is obtained by bypassing the shaded modules. This topology can also be reconfigured by evenly distributing the modules into a row-column array resulting in another topology. Therefore SP, BL, TCT and the bypassed and reconfigured (BR) topologies constitute the reconfigurable topologies.

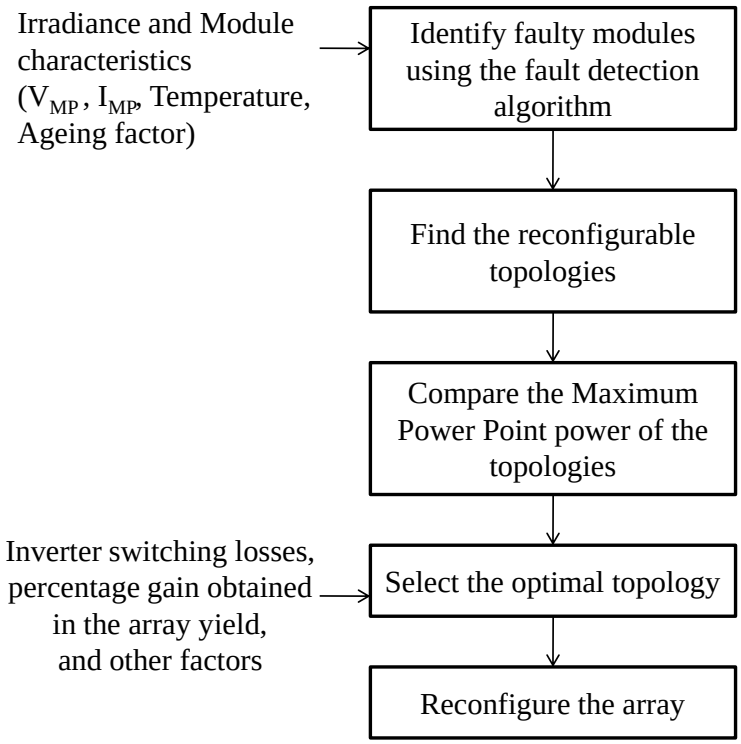

Figure 3.1: Block diagram explaining the topology reconfiguration method.

Performance of the Topologies

Once the reconfigurable topologies are determined, their performance can be predicted using any of the reliable PV models discussed in the Section 2.6. For example, the direct current (DC) power generated by a topology can be determined for a given irradiance (W/m^2) and module temperature (^oC) using the five parameter model in the SPICE simulator. The maximum power point (MPPT) power can be used as a performance metric to compare the topologies. The design of the topologies and procedure to find the MPPT power is explained in the Section 4.1. The MPPT power is expressed as a percentage power obtained with respect to the array power under ideal (no fault) conditions.

Finding the Optimal Topology and Array Reconfiguration

Apart from the MPPT power, other factors are also evaluated to find the optimal topology. These factors include the percentage power gain obtained with respect to the existing topology, the time period before next possible reconfiguration, time of the day, wiring losses and inverter switching losses. The inverter must be turned off during the reconfiguration. This time consumed for the reconfiguration process known as the inverter down time results in losses known as the inverter switching losses. After the analysis of aforementioned factors, the array is reconfigured to the optimal topology using the available reconfiguration facility.

The simulation results that follow in the Chapter 4 consider only MPPT power on the DC side of the inverter to determine the optimal topology. The simulations assume that the connecting wires are ideal while operating. In practice, wiring losses, inverter switching losses, the time period before next possible reconfiguration, and time of the day should be taken into account while implementing array reconfiguration.

Chapter 4

SIMULATION RESULTS

This chapter explains the simulation set-up used to carry out the simulations. The simulation model is validated with the experimental data provided by PACECO company. The behavior of the topologies in the presence of various shading scenarios is presented. The topology reconfiguration method is used to find the best topology for each of the shading patterns. The effect of irradiance and shading on the array performance is studied.

4.1 Simulation Setup

The PV array is designed taking the Sharp NT-175U1 module [42] and the Satcon PowerGate Plus 50KW inverter [43] into consideration. An array of 52 modules arranged in a 13 series, 4 parallel (13x4) configuration is used for the simulations. All the simulations are carried out in the SPICE simulator. The well known single diode model shown in the Figure 2.10 is used to model the photovoltaic module. The current generated by the module is found using the semi-empirical equations given by the five parameter model [1]. The EES solver developed by the University of Wisconsin [29] is used to find the reference parameters. The parameters for a given operating condition are found using the semi-empirical equations.

The circuit diagram representing a photovoltaic module and its symbol used in the simulator are shown in the Figures 4.1 and 4.2. The keyword '.param' is used to define the parameters. The '.model' keyword is used to define the specifications of the diode. The parameters 'Gi' and 'Ti' represent the irradiance (W/m^2) and module temperature (^oC). The rest of the parameters follow the same notation used in [27]. The circuit and symbol used to represent a shaded module are shown in the Figures 4.3 and 4.4. A shaded module receives lower irradiance when compared to a healthy module. The parameter 'Shade factor' represents the percentage of irradiance received by the

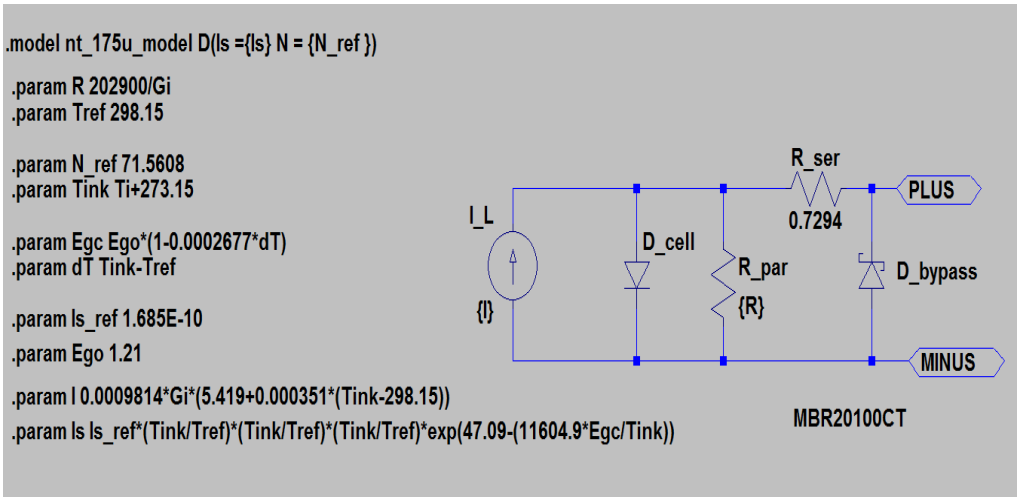

Figure 4.1: Model of the PV module in the simulator

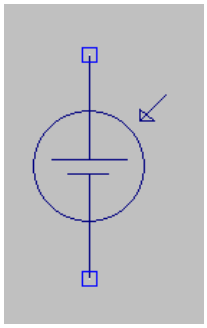

Figure 4.2: Symbol used to represent a PV module in the simulator

shaded module. Therefore the effective irradiance 'Gnew', received by the shaded module is the product of the total irradiance Gi and the shade factor.

The PV module model shown in the Figure 4.1 is used to design the array in SP, TCT and BL topologies as shown in the Figures 4.6, 4.7 and 4.8. The parameters Gi and Ti are given as inputs to the topologies to find the generated DC power. For example, the power-voltage (P-V) characteristic of the SP topology obtained at STC condition (i.e Gi= 1000 W/m^2 and Ti=25 ^oC) is shown in the Figure 4.5. The maximum power point P_{MP} obtained at the maximum power point voltage V_{MP} is shown in the Figure 4.5. Likewise, any topology can be designed using the models for PV module and shaded

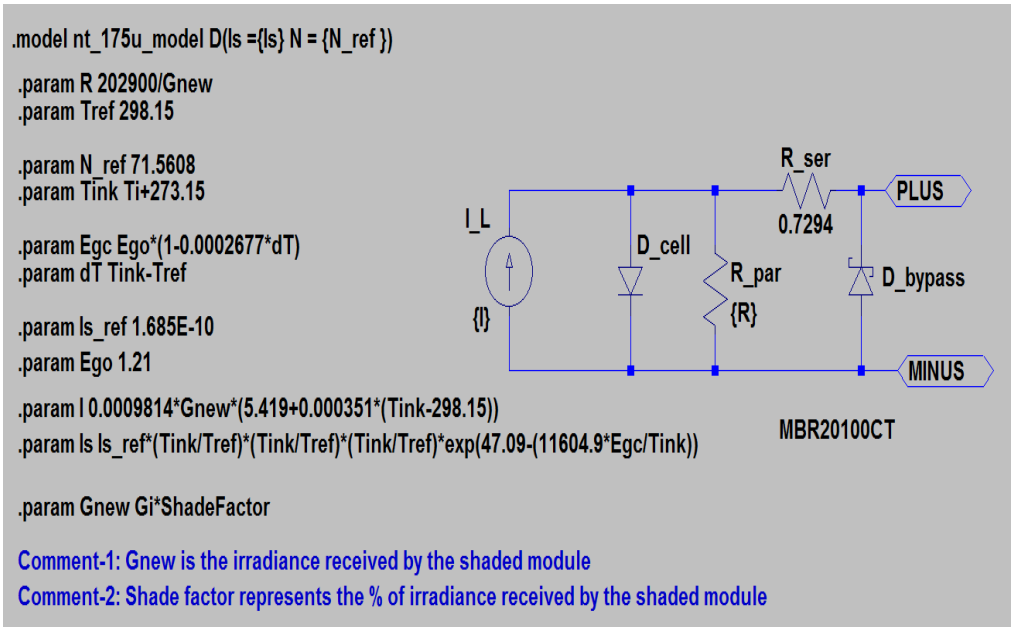

Figure 4.3: Model of the shaded PV module in the simulator

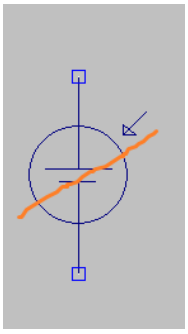

Figure 4.4: Symbol used to represent a shaded PV module in the simulator

module and the DC power can be obtained.

The weather information and module temperatures correspond to Phoenix area for the day May 3rd, 2011 for all the simulations that follow in this chapter. The array performance is found for the day and an average measure is taken to compare the performance of topologies.

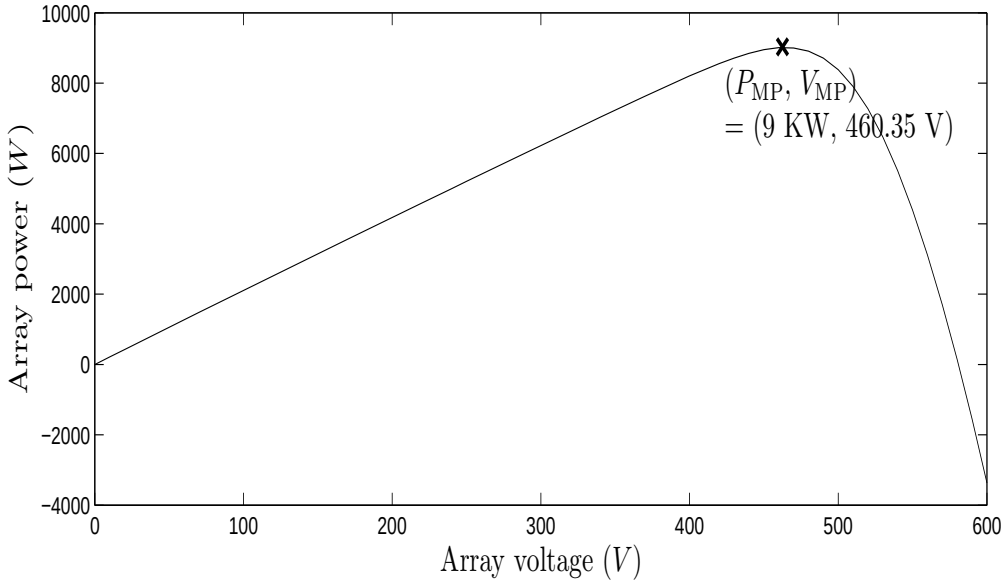

Figure 4.5: Power-voltage characteristic of the SP topology at STC conditions

4.2 Validation of Simulation Results

This section describes the experimental set-up of the PV array followed by comparison of the simulated results with the experimental data.

Experimental Set-up

A grid connected photovoltaic array was set-up in Phoenix by the PACECO company to study the benefits of topology reconfiguration. The array was constructed using the Sharp NT-175U1 modules. An array of 52 modules was considered as it serves as a prototype for large scale grid connected systems. The array was connected to the Satcon PowerGate Plus 50KW inverter. The wiring used for the array was in accordance with the rules imposed by the 2008 United States National Electric Code [36]. Each photovoltaic module was equipped with a node that defines the mode of module connection to the array: series, parallel or bypass. In series and parallel modes, the module is connected in series and parallel respectively with the adjacent module and in bypass mode, the module is bypassed. The array is facilitated with an efficient monitoring system to collect the voltage, current and temperature of the modules and transmit the informa-

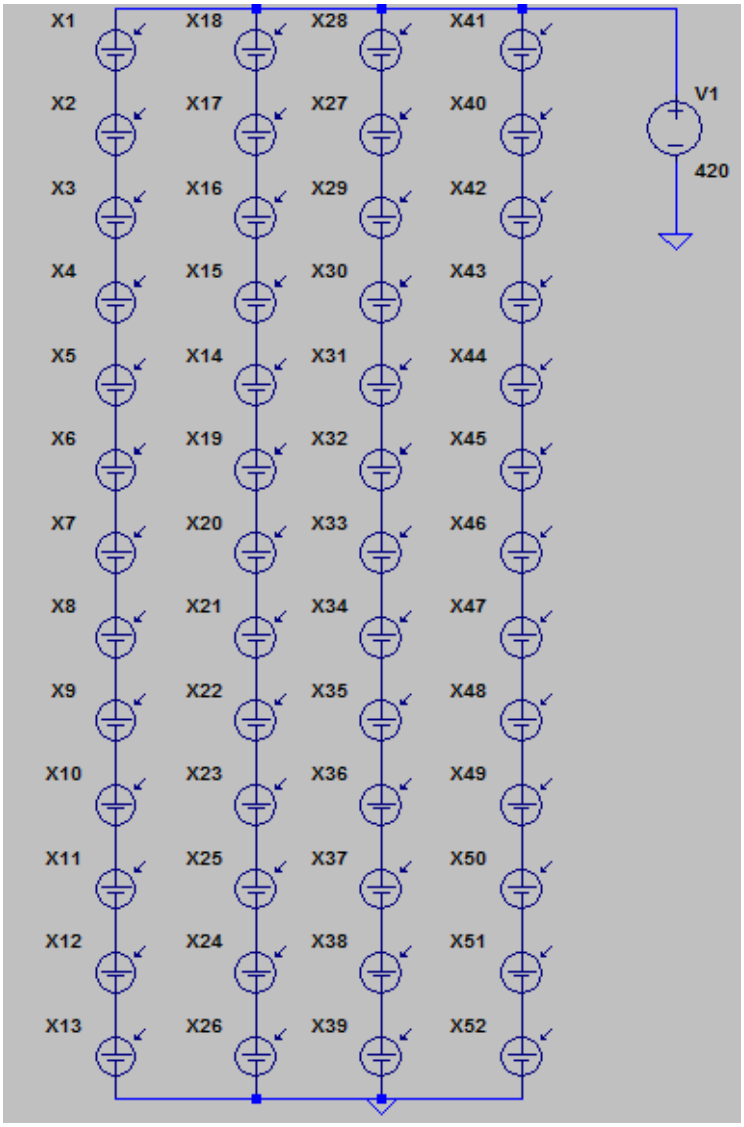

Figure 4.6: Design of series-parallel (SP) topology in the simulator

tion to a server located at the set-up. The weather information (irradiance) collected from weather station is also stored on the server.

Validation

The experimental data for the series-parallel (SP) topology in 13x4 configuration is available from the PACECO company. Array data for two shading tests is available and used to validate the simulation results. In the first test, a single module was shaded

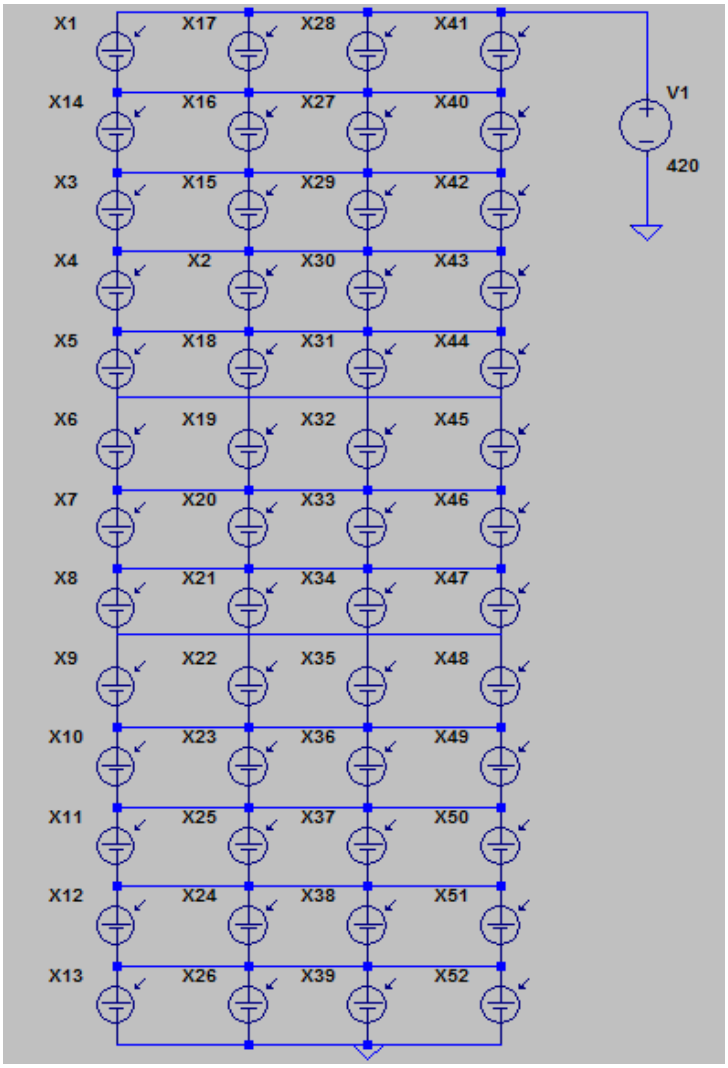

Figure 4.7: Design of total cross-tied (TCT) topology in the simulator

in a string of the array. In the second test, two modules are shaded in a string. A mesh that corresponds to a shade factor of 58.6 % is used to cover the modules and eventually introduce shading. The simulations are performed in SPICE simulator using the provided irradiance and module temperature measurements. The array power is found for the measurements and an average measure is taken. The Figure 4.9 compares the simulated and measured (experimental) results.

From the comparison between the simulated and measured data, it is seen that the simulated results matches closely with the experimental data. The small deviation

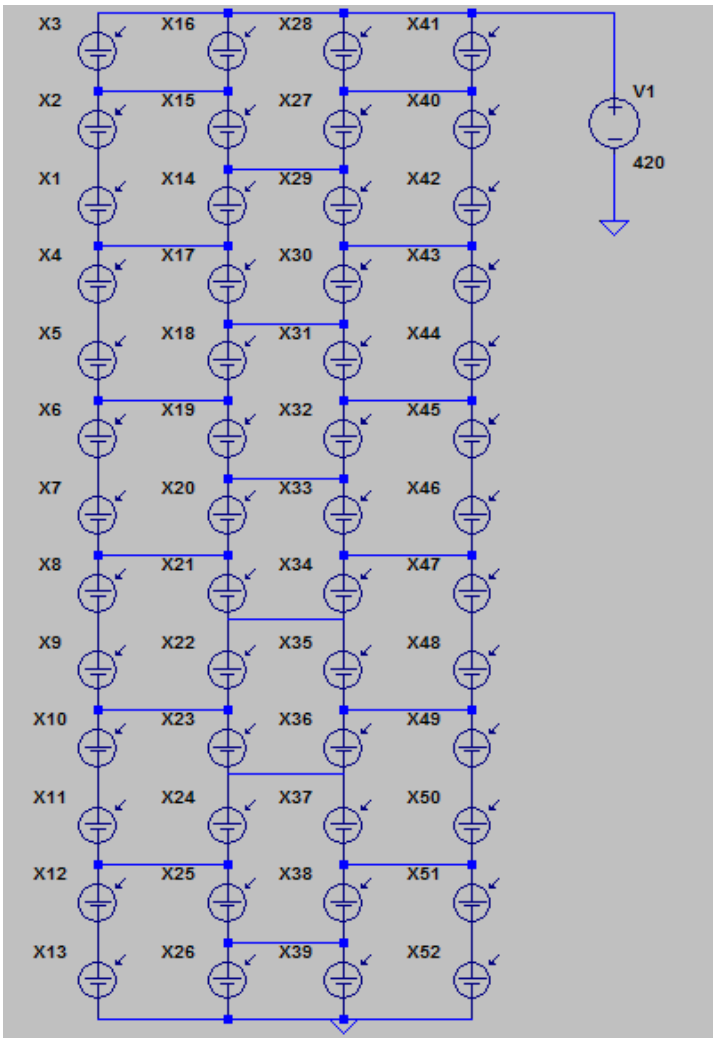

Figure 4.8: Design of bridge link (BL) topology in the simulator

which is around 2 % accounts for the wiring losses and performance degradation of the employed modules due to aging in the real array. In the simulations, wires are assumed to be ideal and modules are expected to perform without any aging effect. These reasons explain the deviation between the measured and simulated data.

4.3 Topology Reconfiguration under Shading

This section applies the topology reconfiguration method to find the optimal topology. The behavior of the topologies for various shading patterns is studied. Here only the MPPT power is used to determine the optimal topology. The array performance is stud-

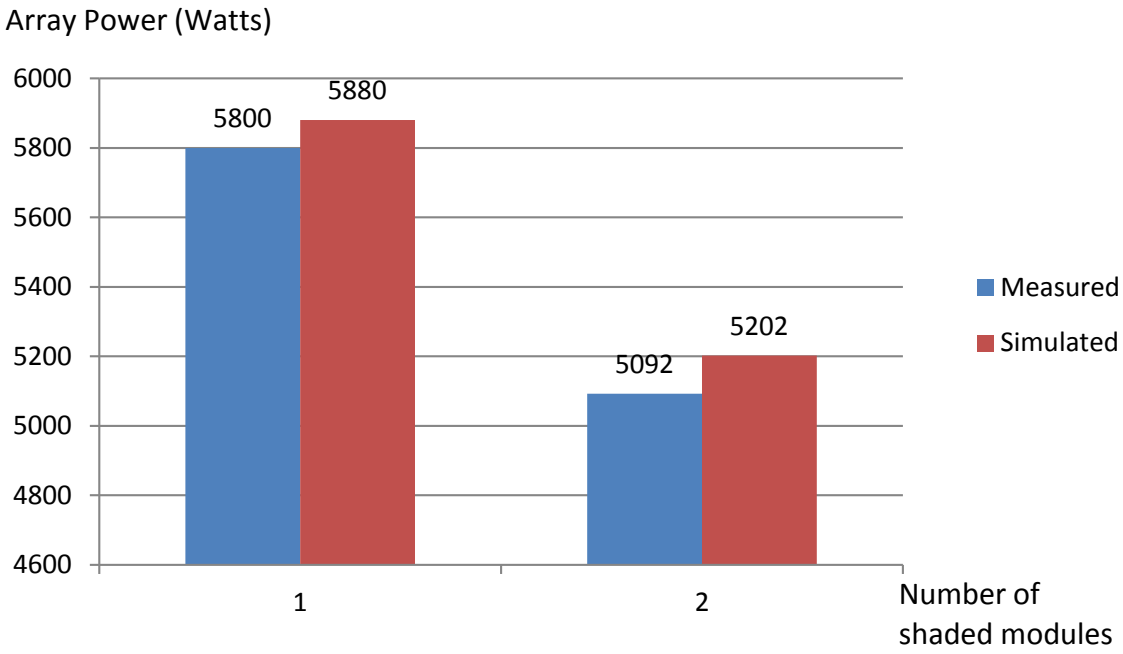

Figure 4.9: Comparison of the measured and simulated data

ied on the DC side of the inverter. So inverter switching losses need not be considered. The array is assumed to have no wiring losses.

Shading Pattern-1

In the first shading pattern, modules are shaded in a single string of the photovoltaic array. This shading pattern is analogous to the shadow caused by trackers, overhead power lines etc. The shading pattern for a SP topology with seven shaded modules is shown in the Figure 4.10. A shade factor of 58.6 % that corresponds to the shade offered by a mesh is considered. It means that the shaded modules receive only 58.6 percent of the overall irradiance incident on them.

Two modules are shaded in the second string of all the topologies. The bypassed and reconfigured topology (BR) is obtained by bypassing the two shaded modules and reconfiguring the array suitably. The number of shaded modules (N) in the second string is increased to 4, 7 and 10 to observe the trend in the performance of the topologies. The topology reconfiguration method is used to find the optimal topology in each

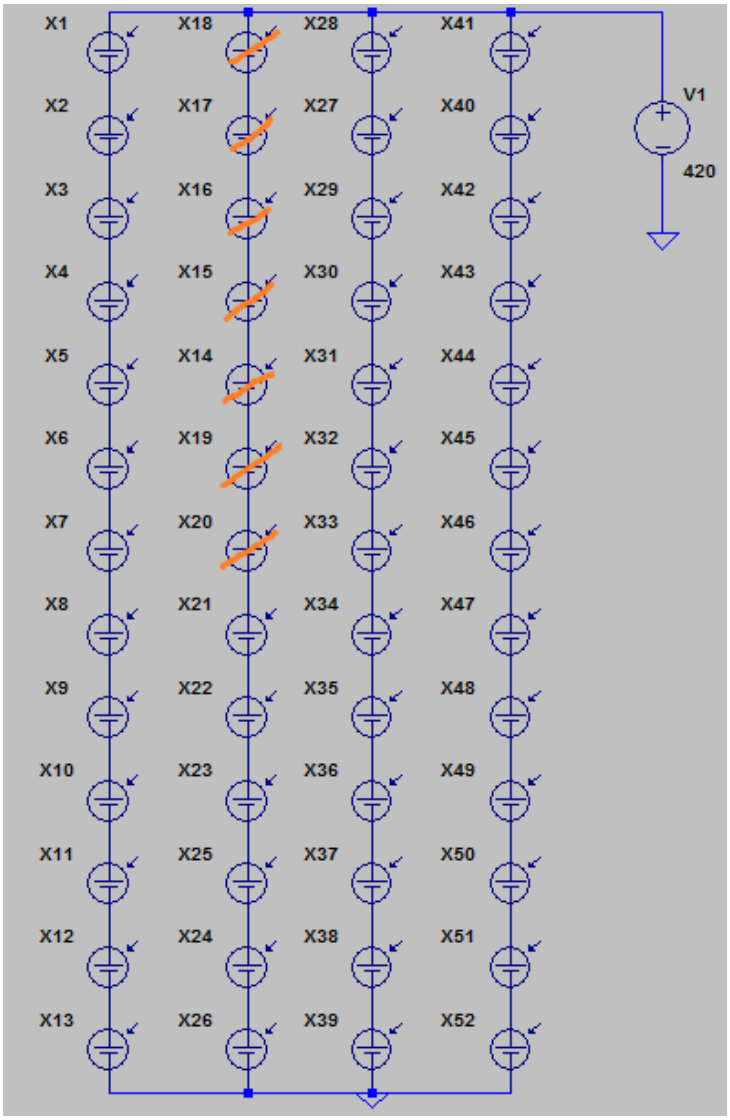

Figure 4.10: Illustration of shading pattern-1.

of the cases. The Figure 4.11 and the Table 4.1 show the percentage output power of the topologies, expressed in reference to the array output under no fault (no shade) conditions.

From the results, it is observed that when there are more than 2 shaded modules, TCT topology performs better than the BL, SP and bypassed and reconfigured topologies. For the two shaded modules case, switching the topology from SP to TCT

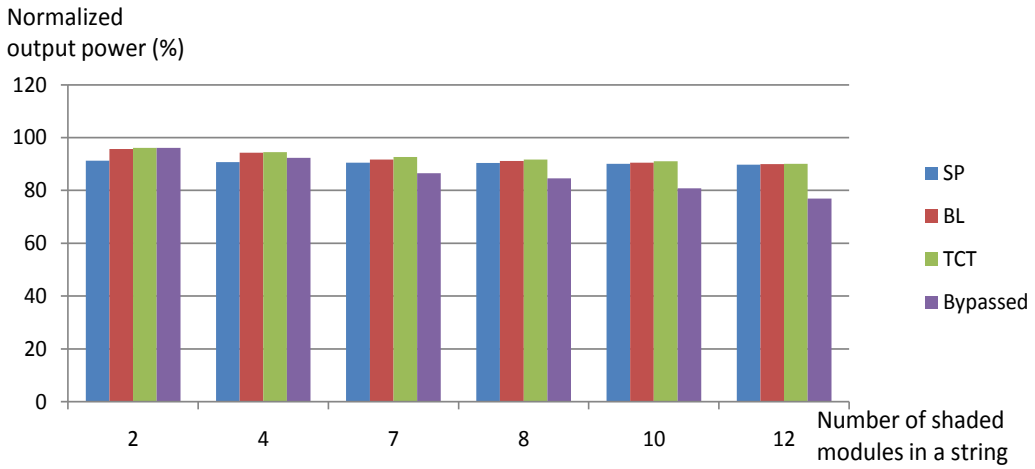

Figure 4.11: Performance of topologies for different number of shaded modules for the shading pattern-1

N	Percentage output power generated by the array			
	SP	BL	TCT	BR
2	91.3	95.7	96.12	96.14 (10x5 SP)
4	90.7	94.2	94.5	92.3 (12x4 SP)
7	90.5	91.6	92.6	86.5 (15x3 SP)
8	90.3	91.1	91.6	84.6 (11x4 SP)
10	90.1	90.4	91.0	80.7 (14x3 SP)
12	89.7	89.9	90.0	76.9 (10x4 SP)

Table 4.1: Performance of the topologies for the shading pattern-1.

and BR topologies results in a % gain of 4.82 and 4.84 respectively in the array output power. Therefore for this shading pattern, bypassed and reconfigured topology (BR) is the optimal topology. But the TCT topology performs better than BR topology as the number of shaded modules increase. Hence TCT topology is considered as the optimal topology for this shading pattern.

Shading Pattern-2

In the second shading pattern, modules are shaded across the strings which is equivalent to the shadow of chimneys, tress etc. The shading pattern for a SP topology with seven shaded modules is shown in the Figure 4.12. Same shade factor of 58.6 % used in the shading pattern-1 is considered.

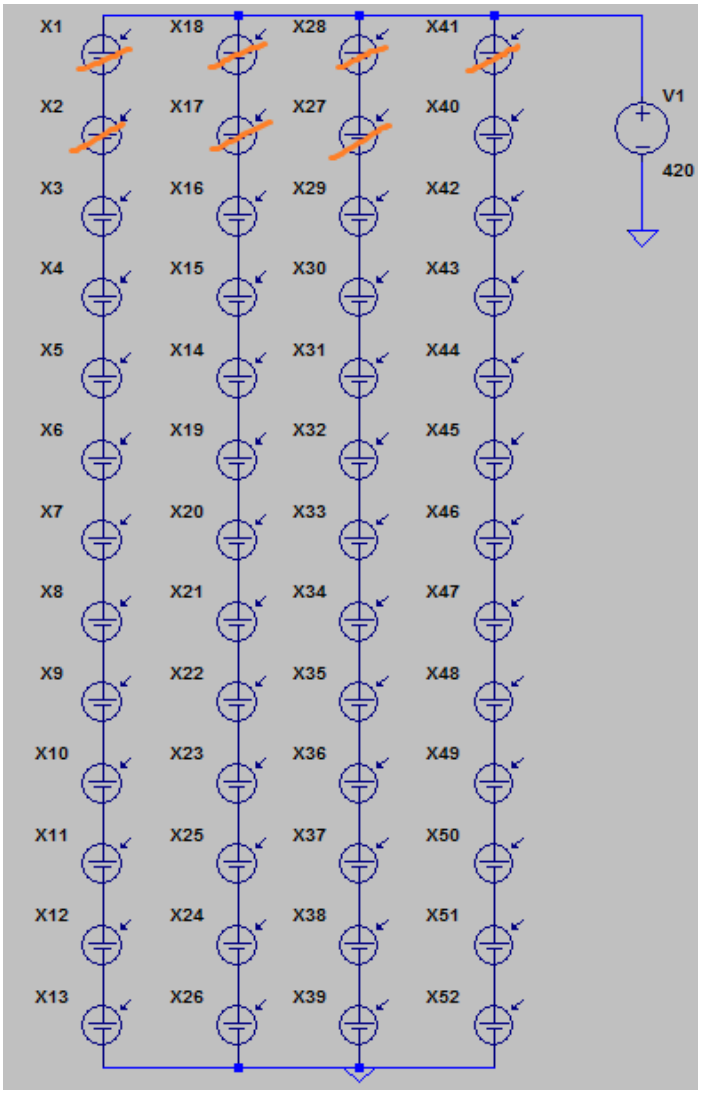

Figure 4.12: Illustration of shading pattern-2.

For example, say seven modules are shaded with two modules each in the first three strings and one in the fourth string. Using the topology reconfiguration method, it is observed that the bypassed and reconfigured topology performs better than the rest of the topologies. It is followed by series-parallel topology which performed better than both the cross tied topologies. Similar result is obtained when ten modules are shaded across the strings: $M(1,1)$, $M(2,1)$, $M(3,1)$, $M(1,2)$ $M(2,2)$, $M(3,2)$, $M(1,3)$, $M(2,3)$, $M(1,4)$ and $M(2,4)$. The results are shown in the Figure 4.13 and the Table

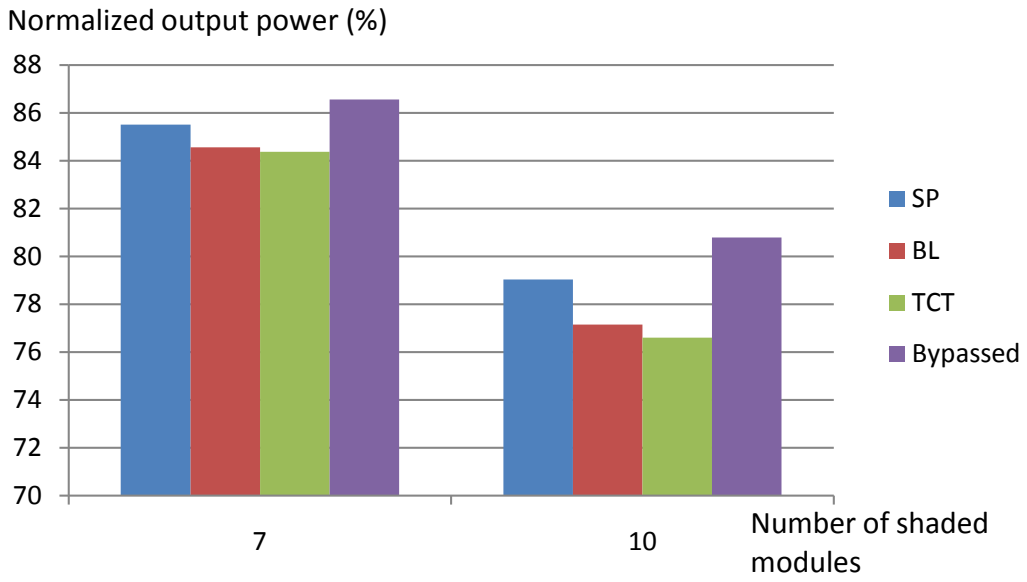

Figure 4.13: Performance of the topologies for the shading pattern-2

N	Percentage output power generated by the array			
	SP	BL	TCT	BR
7	85.5	84.5	84.3	86.5 (15x3 SP)
10	79.0	77.1	76.6	80.7 (14x3 SP)

Table 4.2: Performance of the topologies for the shading pattern-2.

4.2. It is observed for this case that switching the topology from TCT to BR results in a % gain of 4.1 in the array output power. Therefore the bypassed and reconfigured (BR) topology is the optimal topology and reconfiguration of TCT to BR topology would result in a % gain of 4.1 in the array power.

Shading Pattern-3

In this shading pattern, modules are shaded in two strings of the array. The shading pattern for a SP topology with ten shaded modules is shown in the Figure 4.14. A shade factor of 40.0 % is considered.

For example, say ten modules are shaded with nine modules and one module in the first and second strings respectively. The shaded modules are $M(1,1)$ to $M(9,1)$ and $M(1,2)$ in the first and second strings respectively. Similarly twelve modules are

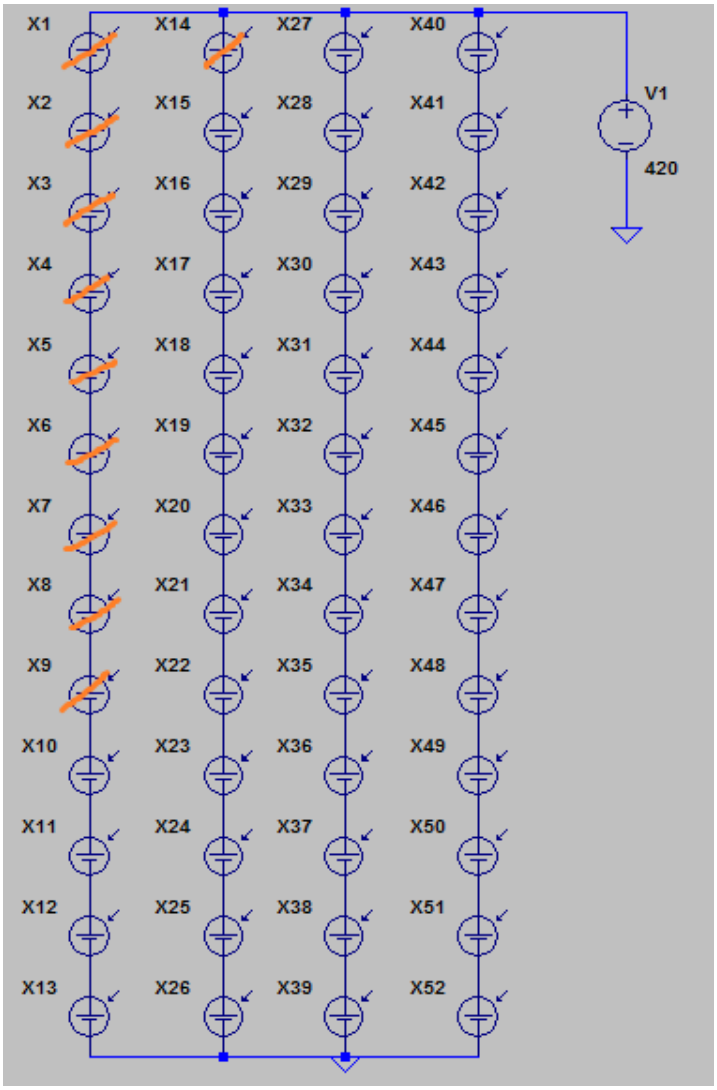

Figure 4.14: Illustration of shading pattern-3.

shaded with nine and three modules in the first and second strings respectively. The modules $M(1,1)$ to $M(9,1)$ and $M(1,2)$ to $M(3,2)$ are shaded. The results are shown in the Figure 4.15 and the Table 4.3.

It is observed that when twelve modules are shaded, switching the topology from SP to TCT and BR topologies results in a % gain of 5.79 and 5.44 respectively in the array output power. This shows that the total cross-tied topology (TCT) is the optimal topology and reconfiguration of SP to TCT topology would result in a % gain

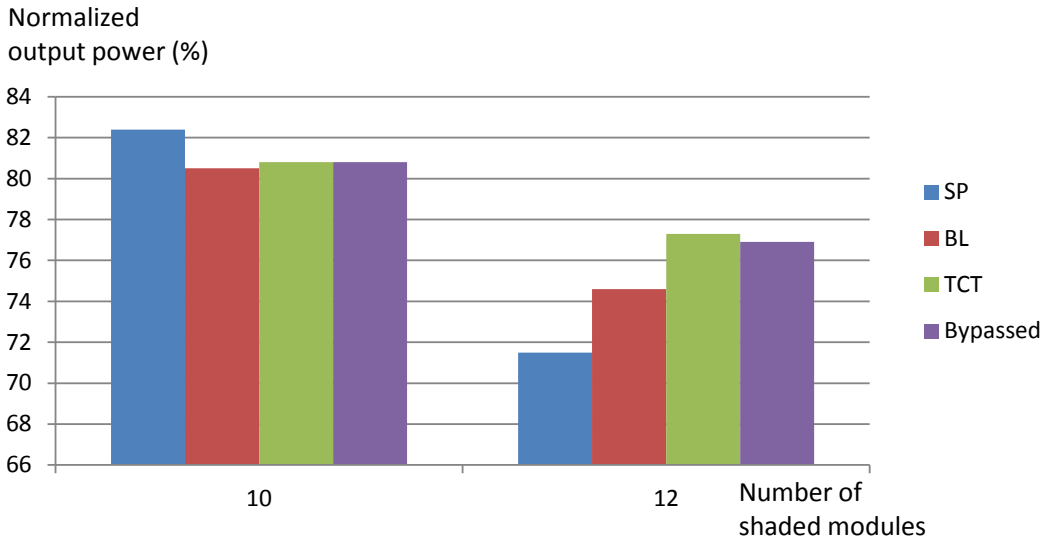

Figure 4.15: Performance of the topologies for the shading pattern-3

N	Percentage output power generated by the array			
	SP	BL	TCT	BR
10	82.4	80.5	80.8	80.8 (14x3 SP)
12	71.5	74.6	77.3	76.9 (10x4 SP)

Table 4.3: Performance of the topologies for the shading pattern-3.

of 5.79 in the array power.

Analysis

From the results, it is clear that the actual pattern of shading determines the topology that is the most optimal. For the first shading pattern, switching from series-parallel to bypassed and reconfigured topology results in a % gain of 4.84 in the array power. Whereas for shading pattern-2, switching from total cross-tied to bypassed and reconfigured topology results in a % gain of 4.1 and for shading pattern-3, a % gain of 5.79 is seen by switching from series-parallel to total cross-tied topology. Therefore from the simulation results, reconfiguration of topologies under shading resulted in an increase in the array power by 4 to 6 %. There can be a different shading pattern producing higher yield compared to the results obtained in this work. Hence a topology reconfiguration method and facility to reconfigure the photovoltaic array would improve the

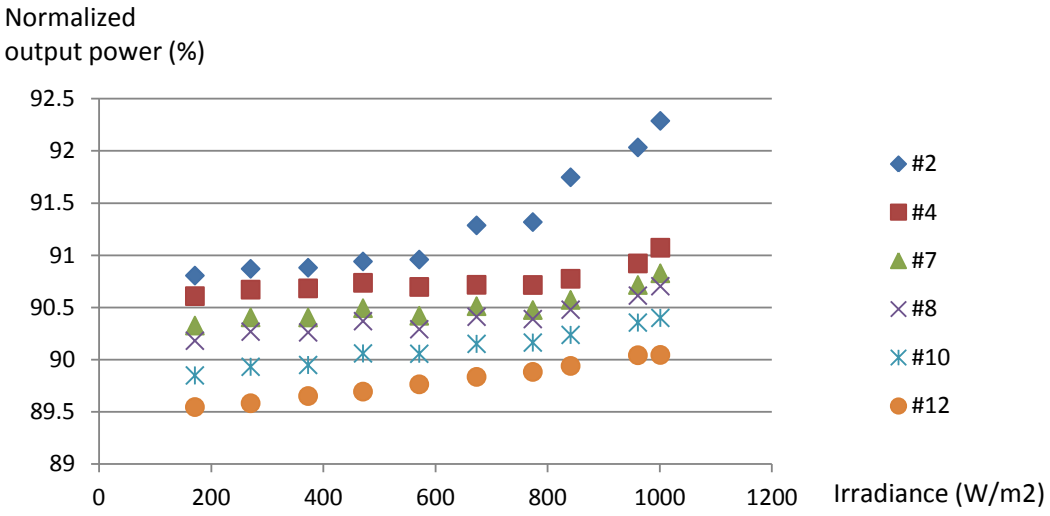

Figure 4.16: Effect of Irradiance on the performance of SP topology

yield from the photovoltaic array.

4.4 Effect of Irradiance on the Array Performance

The effect of irradiance on the performance of the topologies is studied by varying number of shaded modules. The shading pattern shown in the Figure 4.10 is considered. The shaded modules are progressively increased from 2 to 12. The irradiance values fall in the range 100 to 1000 W/m^2 . So, both the lower and higher irradiance scenarios are taken into account. The array behavior of the series-parallel(SP), total cross-tied (TCT), and bridge link (BL) topologies is studied and the results are shown in the Figures 4.16, 4.17 and 4.18. For all the topologies, it is observed that the percentage loss in array power for a given number of shaded modules does not vary much with respect to irradiance. For a given number of shaded modules, the maximum percentage deviation in any of the topologies is 1.5 %. Similar results are obtained irrespective of the shade factor and the type of shading pattern.

4.5 Effect of Intensity of Shading on the Array Performance

The effect of intensity of shading is studied by progressively increasing the shade factor from 10 to 100 % to include the possible range of shading. The performance of series-

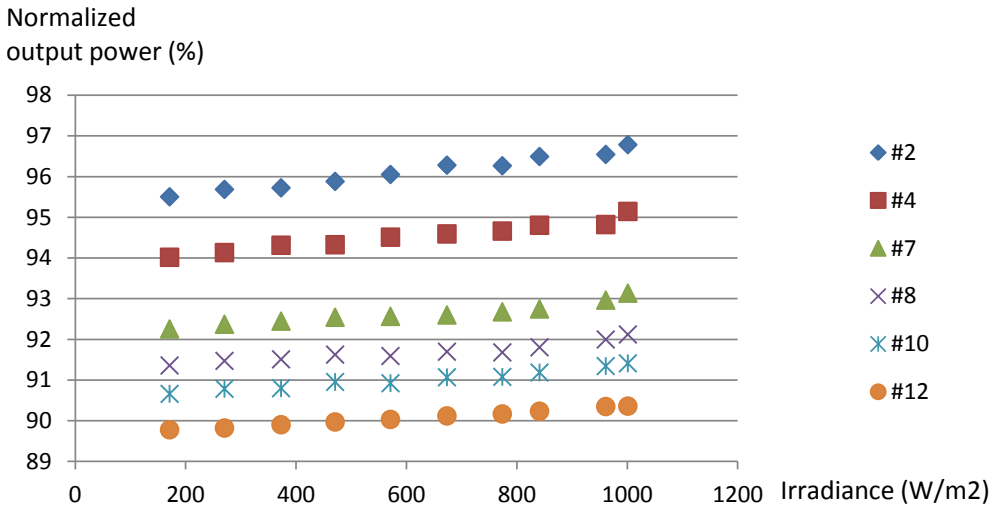

Figure 4.17: Effect of Irradiance on the performance of TCT topology

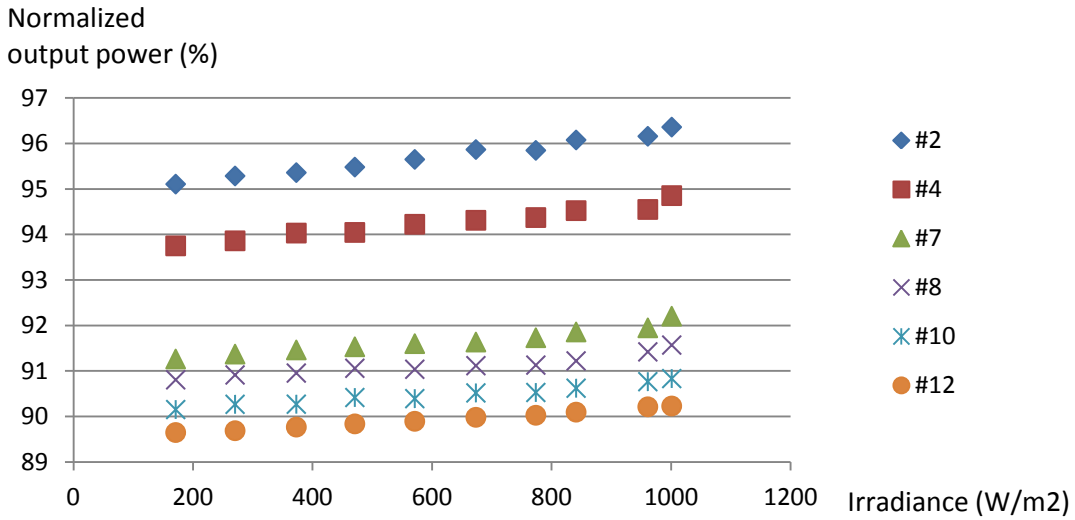

Figure 4.18: Effect of Irradiance on the performance of BL topology

parallel, total cross-tied and bridge link topologies is found for the various feasible shading patterns containing five shaded modules. The optimal topology for each of the shading patterns is analyzed. Five shading patterns are obtained by moving the shaded modules as a cluster. The simulation results, analysis and the generalized results are explained in this section.

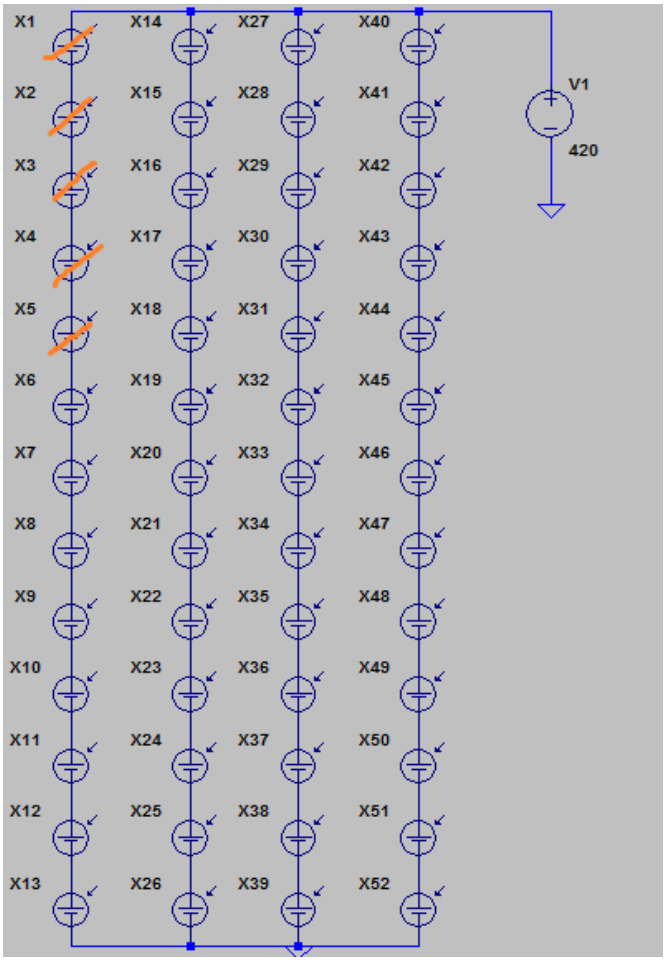

Figure 4.19: Illustration of shading pattern (a).

Simulation Results

The shading pattern (a) shown in the Figure 4.19, consists of shaded modules present in a singe string. The performance of the topologies for the various shade factors is found and the percentage output power generated by the array with reference to the array power at ideal conditions is tabulated in the Table 4.4. It is observed from the results that total cross-tied topology performs consistently better than the other topologies. Therefore, TCT is the optimal topology for this shading pattern.

The shading pattern (b) shown in the Figure 4.20, consists of four shaded mod-

Shade factor	Percentage output power		
	SP	TCT	BL
10	77.7	83.5	82.6
20	80.4	85.8	85
30	83.1	88.1	87.3
40	85.8	90.2	89.5
50	88.4	92.2	91.7
60	91.1	94.2	93.9
70	93.7	96.1	95.8
80	96.3	97.6	97.5
90	98.5	98.9	98.9
100	100	100	100

Table 4.4: Performance of the topologies for the shading pattern (a).

Shade factor	Percentage output power		
	SP	TCT	BL
10	75.3	77.6	77.2
20	77.3	79.6	79.4
30	79.9	81.7	81.5
40	82.5	83.8	83.7
50	85.1	85.7	85.7
60	87.7	89.4	88.2
70	90.3	93.2	92.4
80	93.4	96.4	95.9
90	97.9	98.7	98.7
100	100	100	100

Table 4.5: Performance of the topologies for the shading pattern (b).

ules in the first string and one shaded module in the second string. From the tabulated results in the Table 4.5, it is observed that total cross-tied topology performs consistently better than the other topologies. Therefore, TCT is the optimal topology for this shading pattern.

In the shading pattern (c) shown in the Figure 4.21, the shaded modules are spread across all the strings. From the tabulated results in the Table 4.6, it is observed that series-parallel topology performs better for all the shade factors except for the ones with 60, 70, 80 and 90. For these cases TCT topology performs slightly better than the SP topology. But, the percentage gain that would be obtained by reconfiguring

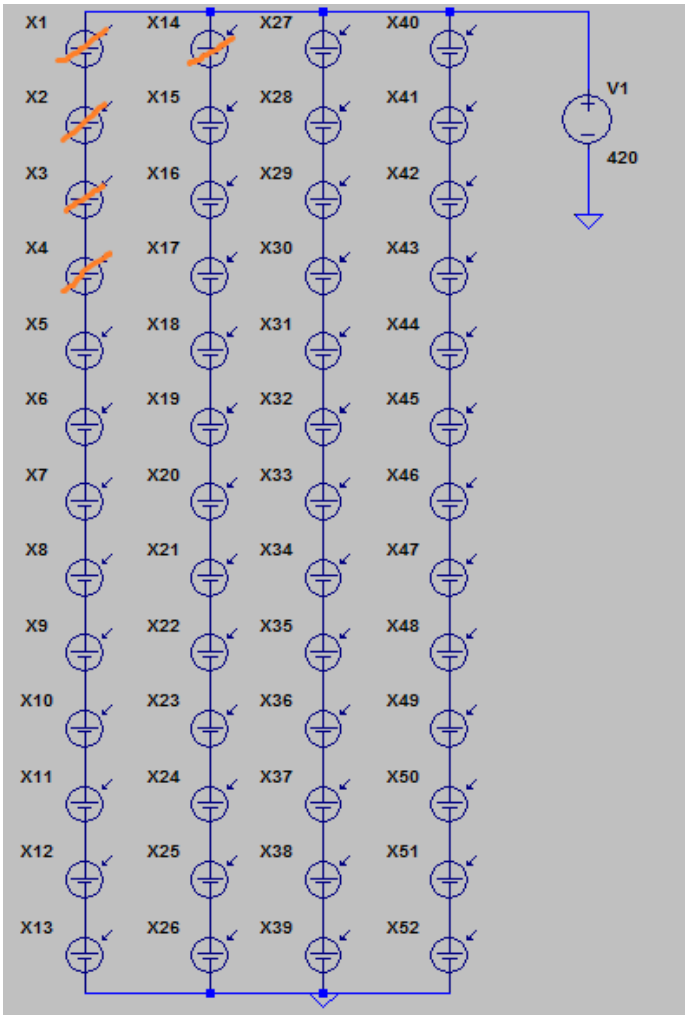

Figure 4.20: Illustration of shading pattern (b).

the topology from SP to TCT for these cases is small compared to the other cases. Therefore, SP topology is considered as the optimal topology for this shading pattern.

In the shading pattern (d) shown in the Figure 4.22, the shaded modules are spread across three strings of the array. From the tabulated results in the Table 4.7, it is observed that series-parallel topology performs better for all the shade factors except for the ones with 70, 80 and 90. But, the percentage gain that would be obtained by reconfiguring the topology from SP to TCT for these cases is small compared to the

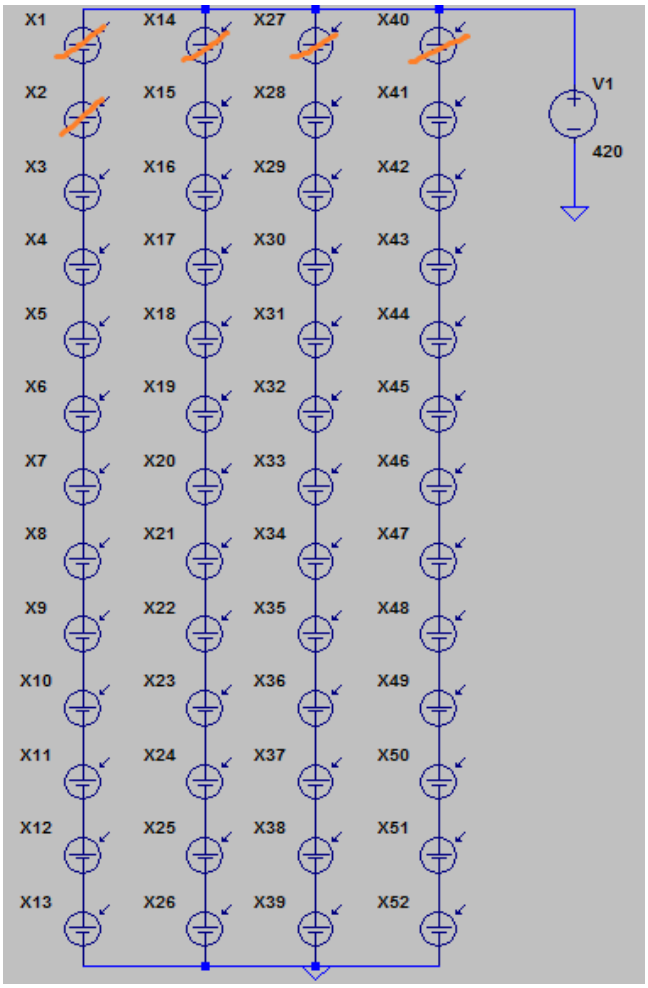

Figure 4.21: Illustration of shading pattern (c).

other cases. Therefore, SP topology is considered as the optimal topology for this shading pattern.

In the shading pattern (e) shown in the Figure 4.23, the shaded modules are distributed across half of the total number of strings in the array. From the tabulated results in the Table 4.8, it is observed that the series-parallel and total cross-tied topologies perform significantly better than the other topologies for lower (10 to 40) and higher (50 to 90) shade factors respectively. Therefore for this shading pattern, either SP or TCT is considered as the optimal topology depending on the intensity of shading.

Shade factor	Percentage output power		
	SP	TCT	BL
10	88.9	84.4	85.7
20	88.9	84.4	85.7
30	88.9	84.9	85.7
40	88.9	86.7	85.7
50	89	88.1	86.6
60	89	89.7	88.3
70	89	90.7	89.7
80	89.7	91.6	91.1
90	97.1	97.2	97.1
100	100	100	100

Table 4.6: Performance of the topologies for the shading pattern (c).

Shade factor	Percentage output power		
	SP	TCT	BL
10	87.3	84.4	84.6
20	87.3	84.4	84.6
30	87.3	84.4	84.6
40	87.3	84.4	84.6
50	87.3	84.4	84.6
60	87.3	84.4	84.6
70	87.3	87.5	87.1
80	91.2	93.5	93.3
90	97.4	98.3	98.2
100	100	100	100

Table 4.7: Performance of the topologies for the shading pattern (d).

Analysis

From the simulation results obtained, it is observed that depending on the shading pattern, either SP or TCT is the optimal topology. The BL topology is always the second best configuration. A percentage gain of 4 to 6 % is noticed when array topology is switched between SP and TCT topologies. This justifies the technique of topology reconfiguration in PV arrays.

An analysis of the topology performance for the different shading patterns shows that if the shaded modules are:

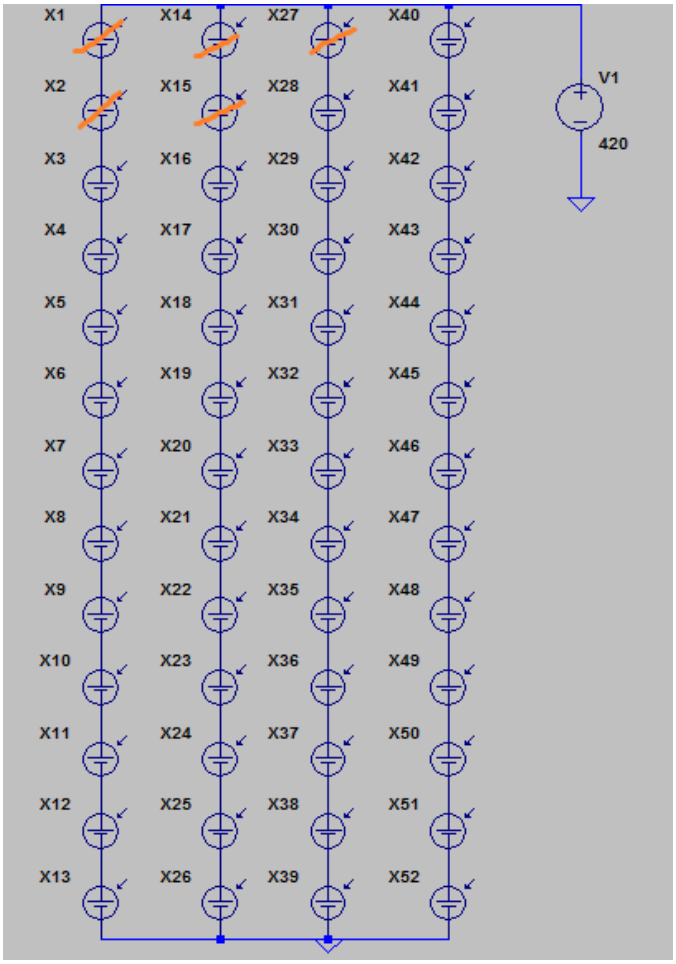

Figure 4.22: Illustration of shading pattern (d).

- localized to a single string, then TCT is the optimal topology.
- spread across all the strings, then SP is the optimal topology.
- distributed across half of the total number of strings in the array, then either SP/ TCT is the optimal topology depending on the intensity of shading.

It is also noticed that shading modules in a single string results in a larger percentage loss in the array power when compared to shading modules across the strings. Therefore, shaded modules when present in a single string is the worst shade pattern

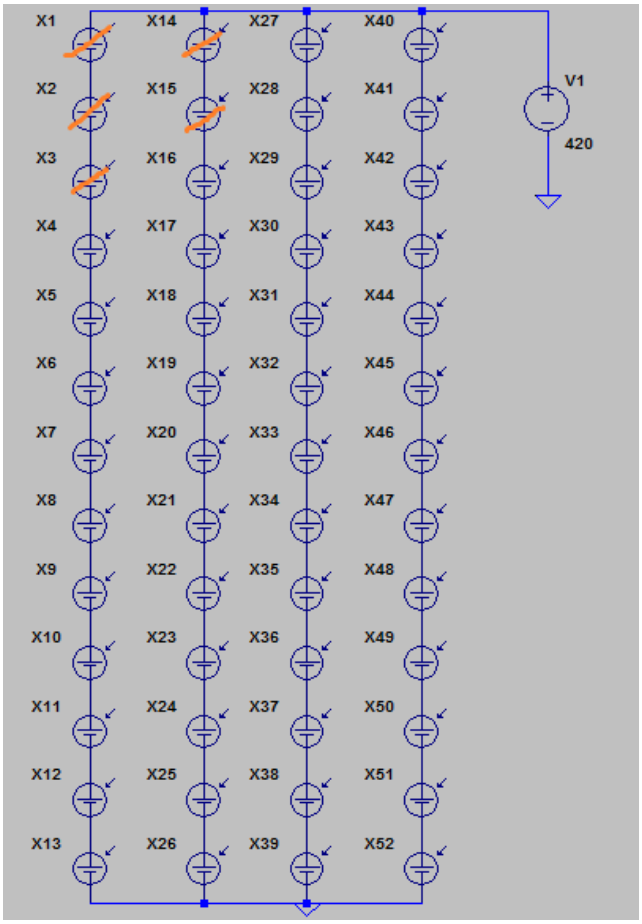

Figure 4.23: Illustration of shading pattern (e).

and shaded modules distributed across the strings is the best shade pattern for the PV array.

Average Performance

In this section, an average measure of the topologies performance is taken to study if any of the topologies would perform consistently better than the others. In reality, the probability of occurrence of shading patterns depend on the physical location, surroundings and, the cloud patterns. If a single topology outperforms the others consistently, then that topology can be fixed for the considered physical location.

The shading patterns shown in the Figures 4.19 to 4.23 represent shade scenar-

Shade factor	Percentage output power		
	SP	TCT	BL
10	82.5	76.5	77.2
20	82.5	76.5	77.2
30	82.5	77.5	77.2
40	82.5	79.5	78.9
50	82.5	84	83.6
60	82.7	88.7	88.2
70	88.1	92.7	92.3
80	93.3	96.1	95.8
90	97.9	98.7	98.6
100	100	100	100

Table 4.8: Performance of the topologies for the shading pattern (e).

ios that commonly occur on a PV array in practice. They include the shade patterns caused by chimneys, over head trackers , transmission lines and random cloud patterns. As the performance of topologies is found in a simulator assuming zero wiring losses and no manufacturing mismatches between modules, the position of the cluster in the array doesn't cause any difference in the array behavior for a given shading pattern.

Assume that the shading patterns (Figures 4.19 to 4.23) are equally likely. The average performance of the array power of the topologies for the shading patterns is tabulated in the Table 4.9. It is observed that the performance of topologies is similar irrespective of the intensity of shading. This is because one of the topologies is performing significantly better than the other topologies for some shading patterns. So, on an average all the topologies have similar performance.

As mentioned in the beginning of this section, the probabilities of the shade patterns is highly dependent on the physical location of the array and the cloud patterns. For a given array at a location, the array performance of the topologies can be studied over a period of time (few days for example) and the probability of shade patterns can be found. If a particular shade pattern predominantly occurs, then the optimal topology for that pattern can be made as the fixed topology of the array. On the other hand, if the patterns are random, then topology reconfiguration method can be used to find the

Shade factor	Percentage output power		
	SP	TCT	BL
10	82.3	82.47	82.5
20	83.47	83.5	83.6
30	84.8	84.7	84.7
40	86.12	86.2	85.8
50	87.4	87.6	87.1
60	88.7	89.4	88.7
70	90.07	91.8	91.25
80	92.65	94.7	94.45
90	97.72	98.2	98.22
100	100	100	100

Table 4.9: Average performance of the topologies assuming equally likely shading patterns.

performance of topologies and the array configuration can be switched to the optimal topology to get the maximum efficiency from the array.

Generalization of the Results

This section performs a detailed analysis of the array behavior under different kinds of shading patterns. The shading patterns can be broadly classified into three categories, depending on the pattern of shaded modules. The shaded modules can be localized to a single string (refer Figures 4.19 and 4.20), present across all the strings (refer Figures 4.21 and 4.22) and distributed across half of the total number of strings (refer Figure 4.23). Consider an array of size *m*x*n* consisting of *k* shaded modules arranged in one of the possible shading patterns discussed. The array behavior and optimal topology for each of the shading patterns is analyzed below:

- If shaded modules are present in a single string (patterns similar to 4.19 and 4.20), then the TCT topology performs better than SP topology. The reason behind such a result is that the bypass diodes would be activated for a longer period in SP topology resulting in a voltage loss from *k* shaded modules. On the other hand, in TCT, the bypass diodes would be activated for a smaller period due to the additional interconnections available in the TCT topology. These intercon-

nections provide alternate current paths for the healthy modules, reducing the overall loss in the array power.

- If shaded modules (for example k=n) are present across all the strings (patterns similar to 4.21 and 4.22), then the SP topology performs better than TCT topology. The reason is that in SP topology, activation of bypass diodes leads to an effective loss of voltage from one module and the string currents are not affected. This is equivalent to an array of configuration $(m-1)$xn without any shaded modules. Whereas in TCT, the bypass diodes would be activated for a shorter period leading to a pronounced effect on all the string currents due to the shaded modules, reducing the overall array power.

- In the third kind of shading pattern, significant number of shaded modules are present in half of the total number of strings (pattern similar to 4.23). This is a variation of the two shading patterns discussed above. In this case, either SP/ TCT is the optimal topology depending on the intensity of shading. The voltage loss from bypassed shaded modules in SP and current loss due to shaded modules in the strings of TCT determines the best topology.

Chapter 5

CONCLUSIONS AND FUTURE WORK

This chapter presents the conclusions from the work done and proposes future work that can be carried out to ascertain the advantages of topology reconfiguration.

Conclusions

The topology reconfiguration method presented in this research is used to find the best topology under shade conditions. The electrical behavior of several topologies such as the series-parallel (SP), the total cross-tied (TCT), the bridge link (BL) and their bypassed versions is studied for various shading situations. For all the cases, the topology reconfiguration method is used to find the best configuration and the percentage gain that would be obtained by switching the topologies is analyzed. The simulation results show that the actual pattern of shading determines the topology that is the most optimal. When shaded modules are in a single string of the array (shading pattern-1), switching from series-parallel to bypassed and reconfigured topology results in a % gain of 4.84 in the array power. With shaded modules distributed across all the strings (shading pattern-2), switching from total cross-tied to bypassed and reconfigured topology results in a % gain of 4.1. Whereas when the shaded modules are present in two strings of the array (shading pattern-3), a % gain of 5.79 is seen by switching from series-parallel to total cross-tied topology. There can be a different shading pattern producing higher yield compared to the results obtained in this work. Also, the percentage gain obtained by array reconfiguration, though appears to be smaller might result in a significant amount of power for large-scale grid connected photovoltaic arrays. Therefore a topology reconfiguration method and facility to reconfigure the photovoltaic array would improve the yield from the photovoltaic array.

The effect of irradiance on the array behavior is analyzed. It is observed that the percentage loss in array power for a given number of shaded modules does not vary

much with respect to irradiance. For a given number of shaded modules, the maximum percentage deviation in the topologies considered is 1.5 %.

The intensity of shading on the array performance is studied by varying the shade factor in the range 10 to 100 %. From the results, it is observed that TCT is the optimal topology when the shaded modules are present in a single string. If the shaded modules are spread across all the strings, then SP is the optimal topology. For the shading patterns in which the shaded modules are distributed across half of the total number of strings in the array, then either SP/ TCT is the optimal topology depending on the intensity of shading.

Future Work

The simulation results carried out in this research show that array reconfiguration would produce a percentage gain of around $4-6$ % in the array power under shading conditions. But the simulations does not take into consideration: the wiring losses, aging of modules and inverter switching losses. To assure the benefits associated with array reconfiguration, vigorous experiments with the employed topologies must be done for several fault conditions. If the gains correspond to a promising amount of power, then reconfiguration facility can be installed in the existing and upcoming photovoltaic plants, increase their power contribution and hence head toward a renewable world.

[1] W. De Soto, S. Klein, and W. Beckman, "Improvement and validation of a model for photovoltaic array performance," *Solar Energy*, vol. 80, no. 1, pp. 78 – 88, 2006.

[2] J. Conti and P. Holtberg, "Levelized cost of new generation resources in the annual energy outlook 2011," US Energy Information Administration, Tech. Rep., Dec. 2010.

[3] D. King, W. Boyson, and J. Kratochvil, "Analysis of factors influencing the annual energy production of photovoltaic systems," *In Proc. Conference Record of the Twenty-Ninth IEEE Photovoltaic Specialists Conference, 2002.*, pp. 1356 – 1361, 2002.

[4] T. Nordmann and L. Clavadetscher, "Understanding temperature effects on PV system performance," *Proceedings of 3rd World Conference on Photovoltaic Energy Conversion, 2003.*, vol. 3, pp. 2243 –2246, 2003.

[5] D. L. King, J. Kratochvil, and W. Boyson, "Measuring solar spectral and angle-of-incidence effects on photovoltaic modules and solar irradiance sensors," *Conference Record of the Twenty-Sixth IEEE Photovoltaic Specialists Conference, 1997.*, pp. 1113–1116, 1997.

[6] D. King, J. Kratochvil, and W. Boyson, "Photovoltaic array performance model," Sandia National Laboratory, Tech. Rep., 2004.

[7] M. V. Paukshto and K. Lovetskiy, "Invariance of single diode equation and its application," *In Proc. 33rd IEEE Photovoltaic Specialists Conference,2008. PVSC '08.*, pp. 1 –4, 11-16 May 2008.

[8] V. Badescu, "Simple optimization procedure for silicon-based solar cell interconnection in a series-parallel PV module," *Energy Conversion and Management*, vol. 47, no. 9-10, pp. 1146–1158, 2006.

[9] G. Velasco, J. Negroni, F. Guinjoan, and R. Pique, "Irradiance equalization method for output power optimization in plant oriented grid-connected PV generators," *In Proc. 2005 European Conference on Power Electronics and Applications*, p. 10, 2005.

[10] G. Velasco-Quesada, F. Guinjoan-Gispert, R. Pique-Lopez, M. Roman-Lumbreras, and A. Conesa-Roca, "Electrical PV array reconfiguration strategy for energy extraction improvement in grid-connected PV systems," *IEEE Transactions on Industrial Electronics,*, vol. 56, no. 11, pp. 4319 –4331, Nov. 2009.

[11] G. Velasco, F. Guinjoan, and R. Pique, "Grid-connected PV systems energy extraction improvement by means of an electric array reconfiguration (EAR) strategy: Operating principle and experimental results," *In Proc. IEEE Power Electronics Specialists Conference, 2008. PESC 2008.*, pp. 1983 –1988, 15-19 2008.

[12] D. Nguyen, "Modeling and reconfiguration of solar photovoltaic arrays under non-uniform shadow conditions," Master's thesis, Northeastern University, 2008.

[13] D. Nguyen and B. Lehman, "A reconfigurable solar photovoltaic array under shadow conditions," *In Proc. Twenty-Third Annual IEEE Applied Power Electronics Conference and Exposition, 2008. APEC 2008.*, pp. 980 –986, 2008.

[14] D. Picault, B. Raison, S. Bacha, J. Aguilera, and J. De La Casa, "Changing photovoltaic array interconnections to reduce mismatch losses: a case study," *International Conference on Environment and Electrical Engineering*, 2010.

[15] D. Picault, B. Raison, S. Bacha, J. de la Casa, and J. Aguilera, "Forecasting photovoltaic array power production subject to mismatch losses," *Solar Energy*, vol. 84, no. 7, pp. 1301 – 1309, 2010.

[16] N. D. Kaushika and N. K. Gautam, "Energy yield simulations of interconnected solar PV arrays," *IEEE Power Engineering Review,*, vol. 22, no. 8, pp. 62 –62, Aug. 2002.

[17] N. Kaushika and A. K. Rai, "An investigation of mismatch losses in solar photovoltaic cell networks," *Energy*, vol. 32, no. 5, pp. 755 – 759, 2007.

[18] T. Markvart, *Solar Electricity*, 2nd ed. Wiley, May 2000.

[19] E. Noll, *Wind/solar energy for radiocommunications and low-power electrical systems*. H.W. Sams, 1981.

[20] L. N. Robert L. Boylestad, *Electronic Devices and Circuit Theory*. Prentice-Hall of India Private Limited, 2002.

[21] C. Honsberg and S. Bowden, *PV CDROM*. [Online]. Available: http://www.pveducation.org/pvcdrom.

[22] J. Nelson, *The Physics of Solar Cells*. Imperial College Press, 2003.

[23] A. Jain and A. Kapoor, "A new method to determine the diode ideality factor of real solar cell using lambert w-function," *Solar Energy Materials and Solar Cells*, vol. 85, no. 3, pp. 391 – 396, 2005.

[24] H. Bayhan and M. Bayhan, "A simple approach to determine the solar cell diode ideality factor under illumination," *Solar Energy*, vol. 85, no. 5, pp. 769 – 775, 2011.

[25] G. S. E. Society, *Planning and Installing Photovoltaic Systems : A Guide for Installers, Architects and Engineers*, 2nd ed. Earthscan Ltd, 2007.

[26] W. D. De Soto, "Improvement and validation of a model for photovoltaic array performance," Master's thesis, University of Wisconsin-Madison, 2004.

[27] W. De Soto, S. Klein, and W. Beckman, "Improvement and validation of a model for photovoltaic array performance," *Solar Energy*, vol. 80, no. 1, pp. 78 – 88, Aug. 2006.

[28] G. T. Klise and J. S. Stein, "Models used to assess the performance of photovoltaic systems," Sandia National Laboratories, Tech. Rep., 2009.

[29] "EES solver to find the reference parameters of five parameter model." [Online]. Available: http://sel.me.wisc.edu/software.shtml.

[30] D. Riley, C. Cameron, J. Jacob, J. Granata, and G. Galbraith, "Quantifying the effects of averaging and sampling rates on PV system and weather data," *In Proc. 2009 34th IEEE Photovoltaic Specialists Conference (PVSC)*, pp. 000 456 –000 461, June 2009.

[31] F. Spertino and J. Akilimali, "Are manufacturing I-V mismatch and reverse currents key factors in large photovoltaic arrays," *IEEE Transactions on Industrial Electronics,*, vol. 56, no. 11, pp. 4520 –4531, Nov. 2009.

[32] R. Hammond, D. Srinivasan, A. Harris, K. Whitfield, and J. Wohlgemuth, "Effects of soiling on PV module and radiometer performance," *Conference Record of the Twenty-Sixth IEEE Photovoltaic Specialists Conference, 1997.*, pp. 1121 –1124, 1997.

[33] H. Patel and V. Agarwal, "MATLAB-Based modeling to study the effects of partial shading on PV array characteristics," *IEEE Transactions on Energy Conversion,*, vol. 23, no. 1, pp. 302 –310, Mar. 2008.

[34] D. Nguyen and B. Lehman, "Modeling and simulation of solar PV arrays under changing illumination conditions," *In Proc. IEEE Workshops on Computers in Power Electronics, 2006. COMPEL '06.*, pp. 295 –299, July 2006.

[35] V. Quaschning and R. Hanitsch, "Numerical simulation of current-voltage characteristics of photovoltaic systems with shaded solar cells," *Solar Energy*, vol. 56, no. 6, 1996.

[36] *NFPA 70: National Electrical Code*, NFPA Std., 2008.

[37] G. Gregory and G. Scott, "The arc-fault circuit interrupter: an emerging product," *IEEE Transactions on Industry Applications*, vol. 34, no. 5, pp. 928 –933, 1998.

[38] G. Gregory, K. Wong, and R. Dvorak, "More about arc-fault circuit interrupters," *IEEE Transactions on Industry Applications,*, vol. 40, no. 4, pp. 1006 – 1011, 2004.

[39] M. Naidu, T. Schoepf, and S. Gopalakrishnan, "Arc fault detection scheme for 42-V automotive dc networks using current shunt," *IEEE Transactions on Power Electronics,*, vol. 21, no. 3, pp. 633 –639, May 2006.

[40] H. Haeberlin and M. Kaempfer, "Measurement of damages at bypass diodes by induced voltages and currents in PV modules caused by nearby lightning currents with standard waveform," in *23rd European Photovoltaic Solar Energy Conference*, 2008.

[41] H. Braun, S. T. Buddha, V. Krishnan, A. Spanias, C. Tepedelenlioglu, T. Yeider, and T. Takehara, "Signal processing for fault detection in photovoltaic arrrays," submitted to the IEEE ICASSP 2012.

[42] *Sharp NT-175UC1 datasheet*, Sharp Electronics Corporation, 5901 Bolsa Avenue, Huntington Beach, CA 92647, 2008.

[43] *Satcon PowerGate Plus 50kW datasheet*, SatCon Technology Corporation, 2009.

APPENDIX A

SANDIA PERFORMANCE MODEL

```
function [V I] = get_IV_curve(env)


%set module parameters for Sharp NT-175U panel, Sandia model
function [modelParams arrayParams envParams] = get_params()
clear modelParams %envParams
modelParams.name = 'Sharp NT-175U1';
modelParams.vintage = 2007;
modelParams.area = 1.3;
modelParams.material = 'c-Si';
modelParams.series_cells = 72;
modelParams.parallel_strings = 1;
modelParams.Isco = 5.40;
modelParams.Voco = 44.4;
modelParams.Impo = 4.95;
modelParams.Vmpo = 35.4;
modelParams.aIsc = .000351;
modelParams.aImp = -.000336;
modelParams.C0 = 1.003;
modelParams.C1 = -.003;
modelParams.BVoco = -.151;
modelParams.mBVoc = 0;
modelParams.BVmpo = -.158;
modelParams.mBVmp = 0;
modelParams.n = 1.323;
modelParams.C2 = .001;
modelParams.C3 = -8.711;
modelParams.A = [.931498305 .059748475 -.010672586 .000798468
```

```
  -2.23567E-5];% actual NT-175u parameters
%modelParams.A = [0.921940714 0.070891738 -0.01427241 0.001170898
  -3.37053E-5]; %parameters from other C-Si panel
modelParams.B = [1 -.002438 .0003103 -1.246E-5 2.112E-7 -1.359E-9];
modelParams.dTc = 3;
modelParams.fd = 1;
modelParams.a = -3.56; %actually alpha in King's paper
modelParams.b = -.075; %actually beta
modelParams.C4 = .992;
modelParams.C5 = .008;
modelParams.Ixo = 5.32;
modelParams.Ixxo = 3.51;
modelParams.C6 = 1.128;
modelParams.C7 = -.128;
modelParams.e0 = 1000;
modelParams.To = 25;

%set parameters for De Soto model

% %set environmental conditions:
envParams.airmass = 1;
envParams.aoi = 0; %angle of incidence
envParams.T_ambient = 25;
envParams.T_cell = 30;
envParams.irradiance = 1000;
envParams.P_diffuse = 0;
```

```
%set parameters of the array:

%Array tracking type. 0 for fixed angle, 1 for single-axis,
% 2 for dual-axis.
arrayParams.trackType = 2;

%direction of tilt (maximum decrease) in degrees.
%0 is North, 90 is east.
%ignored for tracking type 2 (dual-axis).
arrayParams.tiltDirection = 180;

%FIXED tilt angle in degrees.  0 is lying flat on the ground,
%90 is standing on edge.  ignored for tracking type 2 (dual-axis).
%For type 1 (single-axis), this is the angle when panels are
%stowed horizontally.
arrayParams.tiltAngle = 15;

arrayParams.size = 72;  %number of modules in array
arrayParams.moduleType = 'Sharp NT-175U1'; %type of module used

%Maximum and minimum voltages before
%inverter shutdown
arrayParams.maxVoltage = 600;
arrayParams.minVoltage = 300;
arrayParams.maxCurrent = 55;  %conductor ampacity at SRC (25 C)

%temperature coefficient of ampacity
```

```
arrayParams.tempCoeffAmpacity = -.85/100;

arrayParams.nSer = 12;
arrayParams.nPar = 6;
arrayParams.resistance = 1;

arrayParams.location.longitude = -111.912186;
arrayParams.location.latitude = 33.423745;
arrayParams.location.altitude = 305; %in meters

arrayParams.utcOffset = -7; %UTC offset in hours

%calculation of a solar panel IV curve based on the Sandia
%performance model.
k = 1.38066E-23; %Boltzmann's constant, J/K
q = 1.602E-19; % charge of electron, coulombs

%calculate airmass dependence of model:
f_airmass = max(0,polyval(fliplr(model.A),env.airmass));

%calculate angle of incidence dependence:
f_aoi = polyval(fliplr(model.B),env.aoi);

%calculate temperature difference from SRC:
delta_T = env.T_cell - model.To;

%calculate short-circuit current Isc
```

```
Isc = model.Isco * f_airmass *
  (f_aoi * env.irradiance + model.fd * env.P_diffuse)/model.e0
  * (1 + model.aIsc*delta_T);

%calculate effective irradiance Ee
Ee = Isc / (model.Isco * (1 + model.aIsc*delta_T));

%calculate maximum-power current Imp
Imp = model.Impo * (model.C0*Ee + model.C1 * Ee^2)
  *(1 + model.aImp*delta_T);

%calculate "thermal voltage" Vt, T_cell converted from C to K
Vt = model.n * k * (env.T_cell + 273.15)/q;

%calculate open-circuit voltage Voc
 %temperature coefficient as function of effective irradiance
BVoc = model.BVoco + model.mBVoc*(1- Ee);
Voc = max(0,model.Voco + model.series_cells*Vt*log(Ee)
  + BVoc * delta_T);

%calculate maximum power voltage Vmp
%temperature coefficient as function of effective irradiance
BVmp = model.BVmpo + model.mBVmp*(1- Ee);
Vmp = max(0,model.Vmpo + model.C2*model.series_cells*Vt*log(Ee)
  + model.C3*model.series_cells*(Vt * log(Ee))^2 + BVmp * delta_T);

%calculate additional currents Ix and Ixx
```

```
Ix = model.Ixo * (model.C4 * Ee + model.C5 * Ee^2)*
  (1 + model.aIsc*delta_T);
Ixx = model.Ixxo * (model.C6 * Ee + model.C7*Ee^2)
  *(1+ model.aImp*delta_T);

%combine points into vectors
V = [0 Voc/2 Vmp (Voc + Vmp)/2 Voc];
I = [Isc Ix Imp Ixx 0];
if V(2) > V(3)
    V = [0 Vmp (Voc + Vmp)/2 Voc];
    I = [Isc Imp Ixx 0];
end
if Voc == 0
    V = 0;
    I = 0;
end
```

APPENDIX B

FIVE PARAMETER MODEL

```
% Set module parameters for Sharp NT-175U panel
modelParams.material = 'c-Si';
modelParams.series_cells = 72;
modelParams.parallel_strings = 1;
modelParams.Isco = 5.40;
modelParams.Voco = 44.4;
modelParams.Impo = 4.95;
modelParams.Vmpo = 35.4;
modelParams.aIsc = .000351;
a0=.931498305;
a1=.059748475;
a2=-.010672586;
a3=.000798468;
a4=-2.23567E-5;

Tc=T+273.15; % converting the given cell temperature into Kelvin
Tc_ref=298.15;
G_ref=1000;
M_ref=1; % M_ref-air mass modifier at the reference temperature

% Reference parameters obtained from the EES software
a_ref=1.838 ;
I0_ref=1.685*10^(-10);
Il_ref=5.419;
Rs_ref=0.7294;
Rsh_ref=202.9;
```

```
% calculation of 'a'
a=(a_ref*Tc)/Tc_ref;

% Finding the vqlue of Eg at the operating conditions
dT = Tc-Tc_ref;
k = 8.617E-5; %eV/K (boltzmann constant)

%set bandgap of material at To:
switch modelParams.material
    case 'c-Si'
        Ego = 1.21;
    case 'mc-Si'
        Ego = 1.21;
    case 'a-Si'
        Ego = 1.6;
    case 'Si-Film'
        disp('no bandgap specified for cell type ''Si-Film''.
              Using default Si bandgap of 1.21 eV');
        Ego = 1.21;
    case 'CdTe'
        Ego = 1.44;
    otherwise
        disp(['no bandgap specified for cell type
              ''' model.material '''.
              Using default Si bandgap of 1.21 eV']);
        Ego = 1.21;
end
```

```
%set bandgap at Tc:
Egc = Ego * (1 - .0002677 * dT);

% calculation of I0
I0=I0_ref*(Tc/Tc_ref)^3*exp((1/k)*(Ego/Tc_ref-Egc/Tc));

% Finding the value of M at the operating conditions
t=0;    % t- zenith angle, assumed as 0
% AM=1/(cos(t) + 0.50572*(96.07995-t)^(-1.6364) ) ;
AM=1;
M=M_ref*(a0+ a1*AM+ a2*(AM^2)+ a3*(AM^3) + a4*(AM^4));

% calculation of Il
Il=(G/G_ref)*(M/M_ref)*(Il_ref + modelParams.aIsc*(Tc-Tc_ref));

% calculation of Rs
Rs=Rs_ref;

% calculation of Rsh
Rsh=Rsh_ref*(G_ref/G);

V=0:0.001:50;
for p=1:length(V)

     func1=@(C)C-Il+I0*(exp((V(p)+C*Rs)/a)-1)+((V(p)+C*Rs)/Rsh);
     [C,fval,exitflag]=fzero(func1,4);
```

```
    I(p)=C;
    if I(p)<0
       I(p)=0;
    end
end

% Finding the MPP voltage and MPP current
power=I.*V;
[~,q]=sort(power,'descend');
mpp_current=I(q(1));
mpp_voltage=V(q(1));

% Plots the I-V characteristic of the PV module
plot(V,I);
```